2013

Launching a Novel fMRI Study of Vocal Learning and Memory Acquisition in the Songbird Model

Rachel Parker
rparker2@wellesley.edu

Launching a Novel fMRI Study of Vocal Learning and Memory Acquisition in the Songbird Model

Rachel L. Parker

Advisor: Nancy H. Kolodny, Chemistry Department

Submitted in Partial Fulfillment of the Prerequisite for Honors in Chemistry

May 2013

Abstract

The zebra finch model for vocal learning and memory acquisition is capable of providing great insight into fundamental cognitive processes due to the many developmental, physiological and genetic similarities humans share with the zebra finch, *Taeniopygia guttata*. This study establishes a protocol for the use of the fast spin echo (FSE) pulse sequence, rapid acquisition with relaxation enhancement (RARE), for applications in zebra finch blood oxygen level dependent (BOLD) functional magnetic resonance imaging (fMRI). Ultimately these methods will provide a venue for non-invasive whole-brain analyses of zebra finch vocal learning on the neuronal level. Imaging data were collected from adult male and female zebra finches raised with both parents. Preliminary data were also collected from a mouse subject and using a water-containing cylindrical phantom.

Experimentation sought to obtain RARE images meeting the following criteria: Scan time must be short enough to capture the BOLD response, images must be free of artifacts, and maximum signal to noise ratio (SNR) and resolution must be attained. These criteria were met through the systematic manipulation of several parameters with known effects on scan time and the various attributes of image quality. Ultimately, high resolution scans of a zebra finch with a 64 x 64 pixel matrix size (pixel size = 0.22 mm) and with a scan time of 8 seconds were achieved with a maximum SNR of 10.08. However, the use of a small field of view sacrificed SNR to attain a small pixel size, and therefore increased resolution.

A preliminary imaging protocol and later, the optimized protocol, were each applied to an fMRI experiment consisting of 40 second alternating blocks of silence and sound. Sound stimuli consisted of a zebra finch song medley played using G-MAX 2000 Gateway external audio speakers. The subject was an adult male zebra finch that had experienced normal song development. Results from the preliminary protocol showed some BOLD activation after image processing. However, the experimental whole-brain data was misinterpreted by the processing software, SPM8. Data from the optimized protocol have yet to be processed. Future work should focus on developing a better understanding of functional image processing. These efforts will contribute to the establishment of future studies of song learning in isolate juvenile zebra finches.

Acknowledgements

First and foremost I would like to thank **Professor Nancy H. Kolodny** for being a phenominally supportive thesis adviser, an exceedingly patient teacher, and an exceptionally caring mentor. Over the past two years as a student in your lab, I experienced a great deal of personal growth both as a student and as an individual. For all the times you pushed me to ask further questions and to understand a complex subject at its foundations, I am grateful. Now, as I prepare to graduate from Wellesley College, I take with me the motivation and curiosity to seek knowledge at its depths as part of my pursuit of lifelong learning.

Thank you to **Professor Sharon Gobes** for her willingness to serve as both my adviser and thesis committee member. I truly appreciate your support of my contributions to your group's overarching study, your mentorship as my introductory neuroscience professor, and your willingness to share your extensive knowledge of zebra finch vocal learning and memory.

Thank you to **Professors Nolan Flynn** and **Mala Radhakrishnan** for your great enthusiasm. You are two of the professors who continually inspired me to pursue chemistry throughout my time at Wellesley. I am so grateful your continued support and guidance as my thesis committee members.

To **Jon Rose**, thank you for your technical support and maintenance of the MRI system. Many thanks to **Pat Carey** and **Val LePage** for taking excellent care of the finches. I also thank **Artem Goloshevsky** from Bruker Biospin Corporation for generously providing his technical expertise of MRI. Without these individuals, this songbird study would have never gotten off the ground. (Pun intended.)

I want to thank my lab mates for their constant enthusiasm and inspiration. In particular, thank you to **Sarah Zemlok '14** and **Cara Borelli '15** for their insight, contributions, and hard work on this study. We've made so much progress and I can't wait to hear what you accomplish next! And congratulations to my fellow seniors **Palig Mouradian**, **Gina White** and **YiLing Dai** for all their hard work – we made it!

Thank you to all the wonderful professors and friends I have met who have truly made my time at Wellesley meaningful. **Natalie Griffin '14**, thank you for your endless support and confidence in and out of lab. Finally, thank you to my parents, **Stephan** and **Lydia Parker**, brother, **David**, and sister, **Sarah**, for the unconditional love and encouragement you have given me from day one.

In acknowledgement of my funding sources for this project, I thank the Susan Todd Horton Class of 1910 Trust.

Table of Contents

Abstract....2
Acknowledgements....3
Table of Contents....4
Table of Abbreviations....6

1 Introduction....7
1.1 MRI Theory....8
Nuclear Magnetic Resonance....8
Image Contrast....15
Pulse Sequences and Image Construction....18
1.2 Functional MRI....22
BOLD Signal....22
Pulse Sequences....24
Experimental Design and Postprocessing....28
1.3 Songbird fMRI....30
Established Human-Songbird Homologies....30
Technical Challenges....34

2 Materials and Methods....39
2.1 Subjects and Subject Maintenance....39
2.2 Magnetic Resonance Imaging....40
2.3 Subject Preparation....40
2.4 Pulse Sequence Determination....43
2.5 MRI Parameters....43
Anatomical Image Acquisition....44
EPI Image Trajectory Measurement with a Cylindrical Phantom....44
EPI Image Acquisition with a Mouse Subject....45
EPI Image Acquisition with a Zebra Finch Subject....46
RARE Image Acquisition with a Phantom Subject....46
RARE Image Acquisition with a Zebra Finch Subject....50
2.6 fMRI Paradigm....57
2.7 Postprocessing....57

3 Results and Discussion....59
3.1 Pulse Sequence and Image Quality Assessment....59
EPI Image Acquisition with a Mouse Subject....59
EPI Image Acquisition with a Zebra Finch Subject....62
RARE Image Acquisition with a Phantom Subject....64
RARE Image Acquisition with a Zebra Finch Subject....71
Summary....79

4 Conclusions and Future Work....81

References……83
Appendices……85
Appendix A: Guide to Sound Stimulus Recording and Construction………86
Appendix B: Guide to Speaker Assembly……89
Appendix C: Guide to Postprocessing (Adapted from SPM8 Manual)……91

Table of Abbreviations

BOLD: blood oxygen level dependent

BOS: bird's own song

dph: days post hatching

CNR: contrast-to-noise ratio

CSE: conventional spin echo

FID: free induction decay

fMRI: functional magnetic resonance imaging

FOV: field of view

FSE: fast spin echo

GE: gradient echo

HVC: high vocal center (zebra finch neuroanatomy)

MLd: lateral mesencephalic nucleus (zebra finch neuroanatomy)

NCM: caudomedial nidopallium (zebra finch neuroanatomy)

NMR: nuclear magnetic resonance

MRI: magnetic resonance imaging

RARE: rapid acquisition with

RF: radiofrequency

SE: spin echo

SNR: signal-to-noise ratio

SPM8: Statistical Parametric Mapping 8 (image processing software)

TE: echo delay time

TR: repetition time

1 Introduction

The study of songbirds centers on a fascination with a unique quality: the predisposition towards auditory-vocal learning. Indeed, while speech is a familiar human characteristic, the ability to acquire learned vocalizations belongs to a select group of organisms that includes songbirds, hummingbirds, parrots, and possibly whales, dolphins and bats.[1] Charles Darwin himself had noticed songbirds' ability to learn, along with numerous developmental parallels that they share with human infants.[2] Since the 1950s, the study of song development has yielded convincing behavioral and physiological parallels to demonstrate that songbird species provide excellent animal models with which to study the neural mechanisms of vocal learning and memory acquisition. Since the zebra finch genome has been sequenced, researchers have found that humans and zebra finches share many genes that contribute to vocal communication.[3] Knowledge of these analogies and homologies is interesting to neuroscientists who seek insight into cognition on the most basic level. From an evolutionary perspective, it is fascinating that such similarities in vocal learning arose separately in two very different evolutionary branches whose common ancestor existed more than 300 million years ago.[2] Furthermore, the comparisons made by the songbird model for vocal learning and memory are valuable in medicine as they relate to the diagnosis and treatment of speech disorders related to autism, stuttering, stroke, and Parkinson's disease, among others.[3]

However, limited work has been done to study the full process of song development at its most fundamental physiological level. Thus, the ultimate goal of this study is to identify the neural processes underlying song development of the zebra finch (*Taeniopygia guttata*) from the moment song is first introduced to an isolate juvenile. The

implementation of blood oxygen level dependent function magnetic resonance imaging (BOLD fMRI) will allow us to study these processes at the neuronal level. Being a non-invasive technique, BOLD fMRI will also permit us to conduct a whole-brain, longitudinal study of each subject's song development. An additional goal of our study has been to remedy the complex distortions that emerge when functional images are acquired from an avian subject. These studies incorporate basic principles of MRI and BOLD fMRI to minimize the susceptibility artifacts caused by the air cavities in the birds' skulls. The following sections are a review of MRI, fMRI and auditory functional imaging's contributions to the study of the songbird model.

1.1 MRI Theory

Magnetic resonance imaging is a highly versatile and advantageous method due to its numerous applications. Its ability to non-invasively produce high-resolution images of body tissues is invaluable with respect to diagnosis and many more areas in research and medicine. This section will review the theoretical concepts underlying the formation of MR signal to construct an image.

Nuclear Magnetic Resonance

Fundamentally, an atom must exhibit nuclear magnetic resonance (NMR) in order to produce signal in a magnetic resonance image.[4] Ultimately, this property of nuclear magnetic resonance relies on "spin," a property of particles such as protons, neutrons and electrons. All atoms containing an odd number of protons or neutrons have a non-zero spin, and are therefore NMR active. While spin is a quantum mechanical property and does

not refer to the classical concept of spinning about an axis, it often implies the movement of charged particles.[4] This result yields both quantum mechanical and classical explanations of NMR, which provide insight into how MR signal is formed.

The Quantum Mechanical Description of NMR

For a charged nucleus with spin, it can be inferred from Faraday's Law of Magnetic Induction that the moving charge generates its own magnetic field. This magnetic field is associated with a magnetic moment, μ, which is proportional to *p*, angular momentum, and γ, the magnetogyric ratio of the nucleus:

$$\mu = \gamma p \qquad \textbf{(1)}$$

Before the start of an experiment, the magnetic moments of the various sample molecules are pointed in random directions. The degenerate spin states of these NMR-active nuclei are quantifiable by the following expression, for which *I* is the spin quantum number assigned to the nucleus:

$$\#\text{ of spin states} = 2I + 1 \qquad \textbf{(2)}$$

However, when the sample is inserted into a magnet, the magnetic moments of the sample nuclei align with and against the instrument's external magnetic field, as shown:

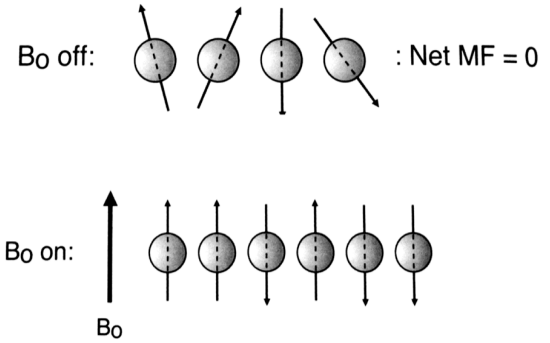

Figure 1-1.[5] When placed inside the magnet of an MRI instrument, sample proton magnetic moments align with and against its external magnetic field, B_0.

The orientation for each nucleus depends on its magnetic quantum number, which has the possible values:

$$m = I, I - 1, I - 2, \ldots - I \qquad \textbf{(3)}$$

For most biologically relevant nuclei, namely ^{1}H, ^{13}C, ^{19}F, and ^{31}P, $I = ½$, which corresponds to two possible spin states, and two observable magnetic quantum states, $m = ½$ and $m = -½$ (Fig. 1-2).[6]

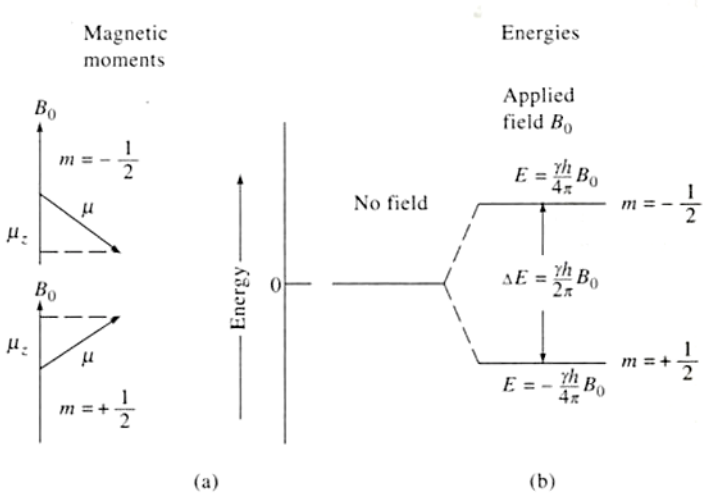

Figure 1-2.[6] (a) Sample nuclei populate two possible magnetic quantum states. (b) When an external magnetic field is applied, the two states lose their degeneracy and are associated with different potential energy levels.

These two observable states are populated based on the Boltzmann distribution, for which N_j is the number of nuclei in the higher energy state, N_0 is the number of nuclei in the lower energy state, ΔE is the potential energy difference between the two states, k is Boltzmann's constant and T is temperature in Kelvin:

$$N_j/N_0 = \exp(-\Delta E/kT) \qquad \textbf{(4)}$$

Being in a less favorable configuration, the nuclei whose magnetic moments are in an antiparallel configuration with respect to the external magnetic field occupy the higher

energy state. This population tends to be very slightly smaller than the population of nuclei whose magnetic moments are aligned with the external magnetic field of the MRI. For this reason, in order to obtain significant signal in a magnetic resonance image, it is essential to acquire signal from an isotope with both high natural abundance and high biological abundance. Because the human body is composed of approximately 60% water, and ^{1}H has a 99.985% natural abundance, hydrogen is the element of choice for the majority of MRI experiments seeking physiological information.[5,7] Sample nuclei are commonly assumed to belong to hydrogen atoms and can be referred to as protons unless otherwise specified.

Signal is produced when sample nuclei are irradiated at their characteristic *Larmor frequency*, which corresponds to the energy difference between the two spin states. At this moment, nuclei in the low-energy spin state are temporarily excited to the high-energy spin state, changing the net magnetization of the sample, the vector sum of the sample nuclei's magnetic moments. The subsequent relaxation is then detected and interpreted as NMR signal. The Larmor frequency, ν_0, is shown in equation **(5)**. Larmor frequency is also commonly expressed in terms of angular frequency, as in equation **(6)**.

$$\nu_0 = \gamma B_0/2\pi \quad \textbf{(5)} \qquad\qquad \omega = \gamma B_0 \quad \textbf{(6)}$$

The Classical Mechanical Description of NMR

In the classical model for NMR, the Larmor frequency also refers to the rate at which the magnetic moments of sample nuclei precess about the axis of the instrument's external magnetic field in a circular motion due to the gyroscopic effect (Fig. 1-3).[6]

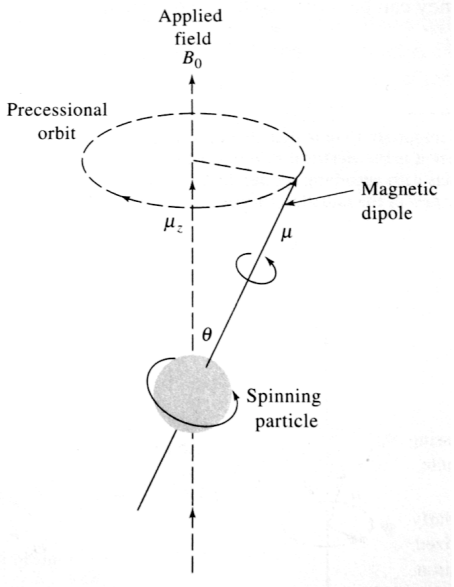

Figure 1-3.[6] Proton precessing about a magnetic field in a gyroscopic motion.

When electromagnetic radiation at the Larmor frequency passes through the sample, the magnetic moments of the sample nuclei align as they tip into the transverse plane (the x-y plane), as shown in Figure 1-4.[8] The pulse of radiation that plays a role in this process is commonly referred to as the "RF pulse" because the Larmor frequency is in the radiofrequency range of electromagnetic radiation.

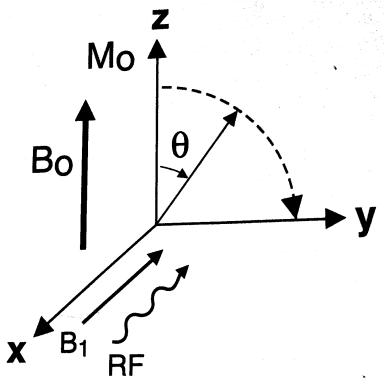

Figure 1-4.[5] The RF pulse causes sample magnetic moments to rotate into the transverse plane at a flip angle, α (θ in the figure).

The angle at which the nuclear magnetic moments collectively move towards the transverse plane is called the "flip angle," α, whose magnitude is dependent on γ, the

gyromagnetic ratio, B_1, the magnetic field strength of the RF magnetic field, and t_p, the duration of the RF pulse:

$$\alpha = \gamma B_1 t_p \qquad \textbf{(7)}$$

The MRI instrument is designed such that its detector only measures precessing magnetic moments in the transverse plane. After M_0, or a projection of M_0 when $\alpha < 90^\circ$, rotates into the transverse plane, the RF pulse is switched off. At that moment, all nuclear spin magnetic moments are in phase in the x-y plane, still precessing in a circular motion about the z-axis at the Larmor frequency. These nuclear spin magnetic moments can be represented by the magnetization vector M_{xy}, as shown in Figure 1-5.

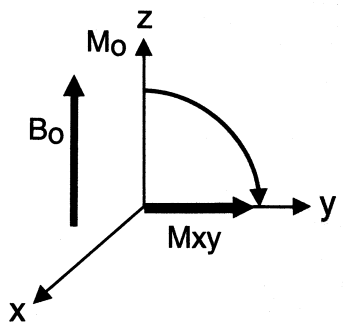

Figure 1-5.[5] When the RF pulse is implemented, the net magnetization vector is in the transverse plane.

Once the RF pulse is turned off, nuclei return to equilibrium, at which they are both in their lowest energy spin states and their magnetic moments are out of phase with each other. The process by the net magnetization vector M_{xy} returns to the z-axis with magnetic field strength M_0 is referred to as the T1 or spin-lattice relaxation. This is analogous to the quantum mechanical concept of nuclei losing the energy imparted to them by the RF pulse, after which they return to the equilibrium Boltzmann distribution of spin states. The rate

of T1 relaxation is dependent on magnetic field strength, and can be expressed in the following equation as M_z recovers to M_0:

$$M_z(t) = M_0(1 - e^{-t/T1}) \quad \textbf{(8)}$$

The entire process lasts up to several seconds (Fig. 1-6).

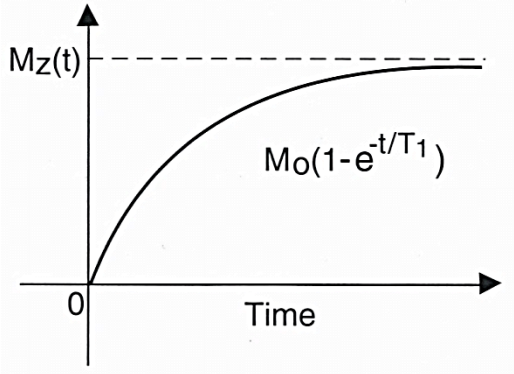

Figure 1-6.[5] Longitudinal magnetization recovery curve represents the change in magnitude of the nuclear spin magnetic moment over time as it relaxes to the z axis.

T2 or spin-spin relaxation refers to the dephasing of nuclear magnetic moments due to external magnetic field inhomogeneities and proton-proton interactions after the end of the RF pulse. As a result, the magnitude of the M_{xy} vector goes to zero by the decay function:

$$M_{xy}(t) = M_0e^{-e/T2} \quad \textbf{(9)}$$

This process lasts on the order of hundreds of milliseconds. It is the T2 relaxation, or more accurately, T2* relaxation that contributes most to the change in signal detected by the RF receiver coil. T2* differs from T2 decay because it relies both on spin-spin interactions and changes in the external magnetic field. It can be mathematically related to T2 relaxation in the expression: $1/T2^* = 1/T2 + \gamma\Delta B$. The RF receiver coil then converts the oscillating magnetic field into current, the signal that can be interpreted by the instrument. The

source of this signal, known as the Free Induction Decay (FID), is the magnetic field vector M_{xy} that is both precessing about the "z-axis" in a sinusoidal motion and steadily decreasing in magnitude as nuclear spins dephase (Fig. 1-7).

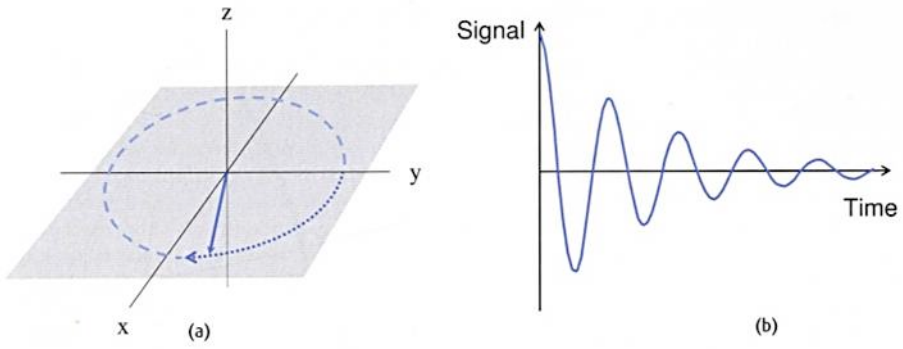

Figure 1-7.[8] The FID originates from the detectable net magnetization vector that oscillates in the transverse plane at the Larmor freuquency after the RF pulse. Its characteristic signal decay is a product of spin dephasing.

FID signal can also be quantified mathematically by the following equation, for which $\cos\omega_0 t$ accounts for the oscillating signal and $e^{-t/T2^*}$ accounts for signal decay:

$$M_{xy}(t) = M_0 e^{-t/T2^*}(\cos\omega_0 t) \quad \textbf{(10)}$$

Image Contrast

One very important point to recognize is that T1, T2 and T2* relaxation times are inherent properties of a material. For an imaging experiment involving a live subject, these relaxation times vary for different tissues and regions in the body depending on the nature of those tissues and the proton density for a given area (Table 1-1). Because of this, T1, T2 and T2* play an important role in determining MRI contrast, allowing us to differentiate between tissues.

Tissue	T1 Relaxation Time (msec)	T2 Relaxation Time (msec)	N(H)
White Matter	**510**	**67**	**0.61**
Gray Matter	**760**	**77**	**0.60**
Edema	**900**	**126**	**0.86**
CSF	**2350**	**180**	**1.00**

Table 1-1.[5] Different tissues containing different numbers of mobile protons, N(H), have inherently different T1 and T2 relaxation times.

Because T1, T2 and T2* relate to the physical properties of the sample, contrast in MRI is typically controlled by regulating how much and when signal is collected.* The two adjustable parameters that can be used to manipulate contrast are the repetition time, TR, and the echo delay time, TE. By definition, TR refers to the time at which an RF pulse is reapplied in an imaging experiment. By repeatedly applying RF pulses (normally 90° pulses), the magnetization vector, M_z, can be prevented from returning to the z-axis, at which signal cannot be detected and $M_z = M_0$ (Fig. 1-8). In other words, reducing TR enhances signal in the transverse plane due to the T1 effect, spin relaxation. Images that primarily incorporate signal due to the T1 effect are known as T1-weighted images.

* Chemical contrast agents can also be used to change the T1, T2 and T2* relaxation times for a sample.

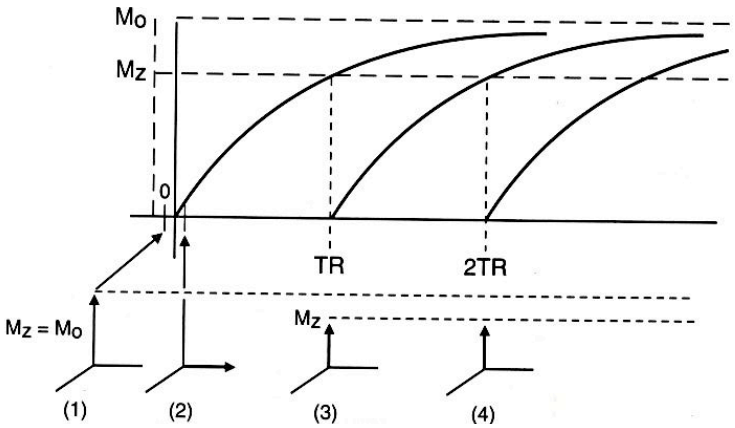

Figure 1-8.[5] A vector component of M_{xy} is maintained in the transverse plane by implementing an RF pulse at each TR. In doing so, a detectable MR signal is maintained.

In the best-case scenario, if FIDs are measured immediately after each TR interval, then maximum signal will be collected (Fig. 1-9). However, the instrument is limited by the time it takes to apply magnetic field gradients. As a result, there is an adjustable period of time, TE, to record a measurement from the FID, which is called an "echo." After the RF pulse is shut off, spin dephasing begins to occur due to proton-proton interactions as part of the T2 effect. The longer TE is extended, the more signal decay will occur. Therefore, a longer TE results in a more prominent T2 effect. Images that primarily incorporate signal due to the T2 effect are known as T2-weighted images.

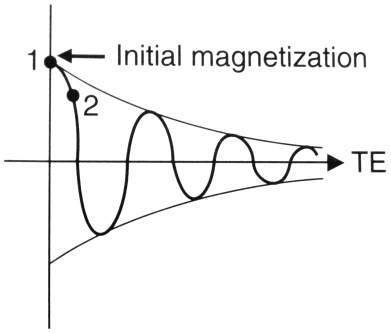

Figure 1-9.[5] MR signal must be collected at a time TE (point 2) after signal due to the initial magnetization decays. This delay is attributable to the time it takes to apply the magnetic field gradients.

In summary, signal intensity can be fully characterized by the following equation, for which SI is signal intensity and N(H) is the number of mobile protons:

$$SI = N(H)(e^{-TE/T2})(1 - e^{-TR/T1}) \qquad \textbf{(11)}^{5}$$

In an imaging experiment, to obtain desirable contrast, it is important to consider:

1. T1 weighted contrast is enhanced with a short TR and a short TE. These parameters allow signal to be collected before the longitudinal magnetizations of nuclear magnetic moments fully recover, and before differences in T2 (transverse magnetization) decay become pronounced.
2. T2 and T2* weighted contrast is enhanced with a long TR and a long TE. This is because these parameters allow for signal to be collected when differences in T1 (longitudinal magnetization) recovery are less pronounced between tissues, and differences in T2 (transverse magnetization) decay rate are more pronounced.

Last, it is important to recognize that good contrast implies relative differences in signal intensities between neighboring tissues. Good contrast can be vital to the success of a study. Without it, healthy tissue and neighboring tumor cells may not be differentiable. (This is just one example.) For this reason, one must choose appropriate TR and TE values that that yield substantial differences in signal intensity among tissues at TE either on the basis of T1 or T2 relaxation times.

Pulse Sequences and Image Construction

A pulse sequence is the predetermined series of radiofrequency and magnetic field gradient pulses timed with a specified TR and TE such that the desired MR contrast is established (Fig. 1-10).

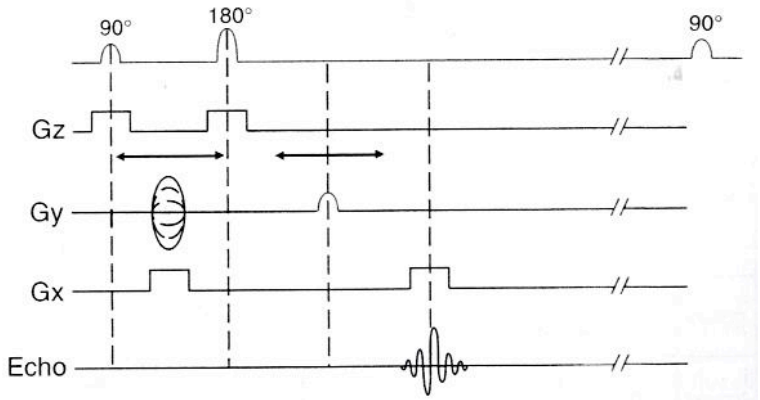

Figure 1-10.[5] Example of a T2-weighted spin echo pulse sequence diagram.

When implemented, a pulse sequence causes signal from every part of the sample to be produced due to the established RF pulses. The function of gradients in MRI is to distinguish between signals that originate from different points in space. This is done by implementing magnetic fields that change linearly along all three axes. In an MRI instrument, there are three different types of gradients that vary depending on their orientation axis and function: G_z, G_x and G_y.

G_z functions as the slice-select gradient in the z direction. By linearly varying the magnetic field in the z direction G_z causes sample protons to precess at differing Larmor frequencies. As a result, G_z impacts which sample protons will produce NMR signal in response to RF pulses. Signal is then received in the form of a slice with a thickness that is related to the "bandwidth" or range of RF frequencies transmitted (Fig. 1-11).

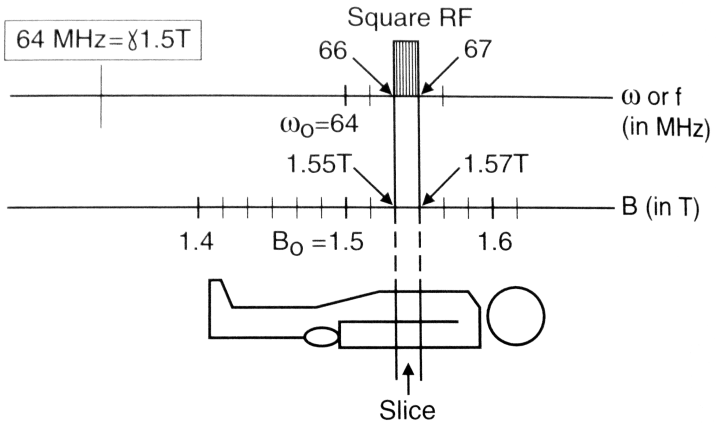

Figure 1-11.[5] The slice select gradient, G_z, determines slice thickness by implementing a magnetic field that varies along the z-axis. Because magnetic field strength is directly related to Larmor frequency, only protons falling within a specific spatial range will match the bandwidth of RF frequencies implemented by the instrument and produce signal.

G_x functions as the frequency-encoding gradient in the x direction. It is applied when signal is received at time TE, and provides information about individual pixels in each slice. When G_x is turned on, it generates a magnetic field that causes sample protons associated with different pixels to precess at different frequencies. Each pixel also contains a different number of protons, which will affect the amplitude of the signal collected. Because each pixel has a unique amplitude and frequency, different positions in space can be easily distinguished. Fourier transform can then be used to convert the signal detected in the frequency domain into spatial information along the x axis.

G_y functions as the phase-encoding gradient in the y direction. G_y is normally implemented somewhere in between the RF pulse and the time G_x is switched on. When G_y is turned on, it creates a magnetic field that causes sample protons to precess at different frequencies depending on their position along the y-axis. Then, when G_y is turned off, the protons return to the Larmor frequency, but out of phase with each other (Fig. 1-12). Signal collected from this process can then be converted from the frequency domain into a spatial distribution by Fourier transform.

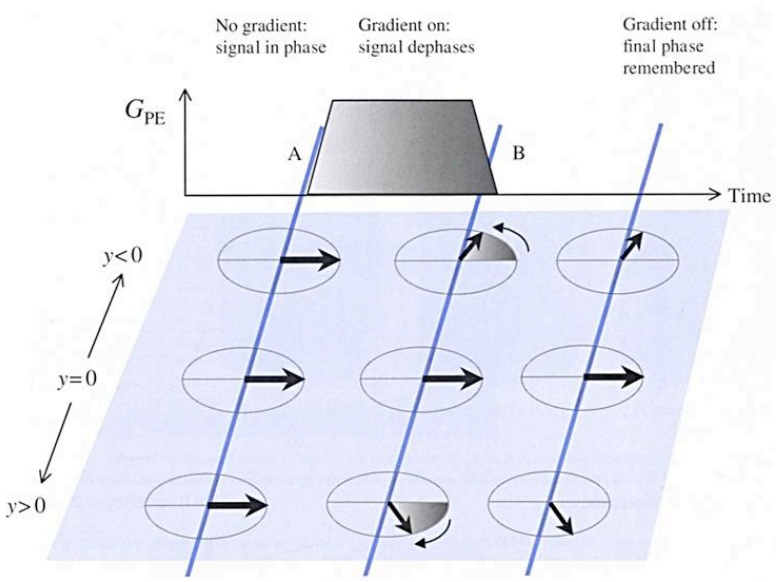

Figure 1-12.[8] The phase encoding gradient, G_y (G_{PE} in the figure), causes sample protons in the y plane to oscillate out of phase, but at the same Larmor frequency.

Altogether, for each TR, G_z, the slice select gradient, is applied during each RF pulse to ensure that a specific bandwidth of protons produces signal. G_y is turned on immediately before an echo, and also in between 90˚ and 180˚ pulses for SE pulse sequences to ensure that protons are resonating out of phase along the y axis when G_x is applied during signal collection. G_x, like G_y, causes protons to precess at different frequencies at different points in space along the x axis and is turned on between the 90˚ and 180˚ pulses during spin echo pulse sequences (Fig. 1-10).[5] Each signal corresponding to a different phase shift fills a different line in a set of digitized rows referred to as k-space (Fig. 1-18). From k-space, signal encoded in the frequency domain can be reconstructed by Fourier transform to produce an image.

1.2 Functional MRI

Functional MRI (fMRI) is a powerful imaging technique, as it allows the non-invasive measurement of neuronal activity in response to a stimulus. This section will review the fundamental concepts and methodologies relevant to acquiring a functional magnetic resonance image.

BOLD Signal

Blood oxygen level dependent (BOLD) functional MRI, a method that is almost exclusively reserved for studies of the central nervous system, relies on the changing magnetic properties of hemoglobin in blood to produce BOLD signal. More specifically, BOLD contrast relies on the concept that oxygenated hemoglobin, or oxyhemoglobin, is diamagnetic and therefore has a very weak magnetic effect. Meanwhile, deoxygenated hemoglobin, or deoxyhemoglobin, has unpaired electrons and is paramagnetic. As a consequence, it has a significant magnetic moment, and will affect MR signal.

In a BOLD fMRI experiment, neuronal activation is measured in response to a stimulus. The MR signal elicited by neuronal activity is referred to as the hemodynamic response (HDR). It is characterized by a 1 to 2 second dip in signal caused by a relative increase in deoxyhemoglobin in the active brain region, followed by a robust increase in signal caused by a rapid influx of oxyhemoglobin responding to that area's metabolic demands (Fig. 1-13).[9]

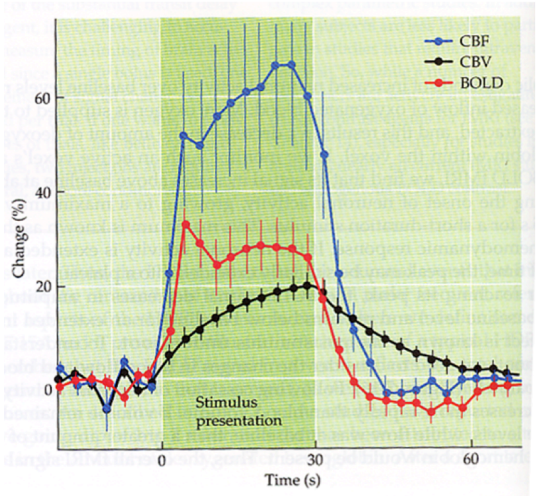

Figure 1-13.[9] Diagram of the hemodynamic response. Data in blue represents % changes in cerebral blood flow (CBF) over time. Data in black represents % changes in cerebral blood volume (CBV) over time. Data in red represents % changes in blood oxygen level dependent (BOLD) signal over time.

The delivery of oxygen quickly exceeds the demand for the active region, leading to a net increase in the blood oxygen level. The substantial influx of oxyhemoglobin decreases the relative concentration of deoxyhemoglobin at the site of neuronal activity. Because relaxation rates (1/T2 and 1/T2*) are proportional to the concentration of magnetically active particles (such as deoxygenated hemoglobin), MR signal in T2- and T2*- weighted images increases with metabolic activity as the overall concentration of deoxyhemoglobin decreases.[10]

Peak HDR, associated with maximum BOLD signal, occurs at approximately 5 seconds after stimulus onset (Fig. 1-13). BOLD signal reaches a plateau following peak HDR for block experiments in which the subject is exposed to multiple stimuli or a prolonged stimulus. After the stimulus is stopped, there is a "poststimulus undershoot" in which BOLD signal is below baseline levels for approximately 20 seconds (Fig. 1-13).[10] This occurs because the rate of cerebral blood flow has returned to normal, while cerebral blood volume in the affected area takes more time to return to baseline. As a result, there is a

greater than average amount of deoxygenated hemoglobin present that causes a reduction in signal.[9]

Pulse Sequences

There are two main scanning methodologies employed in functional MRI: spin echo (SE) and gradient echo (GE) pulse sequences. SE images rely on T2 contrast while GE images rely on T2* contrast. Thus, the objective for a pulse sequence in a functional imaging experiment is to maximize contrast from T2 or T2* relaxation in order to enhance the instrument's sensitivity to the neuronal response.

Echo-planar imaging (EPI), a GE pulse sequence, is the most commonly used fast imaging method due to its short acquisition time and sensitivity to T2* contrast. EPI works on the basic principle that the entirety of k-space can be filled following a single excitation by switching the magnetic field gradients rapidly back and forth (Fig. 1-14).[9]

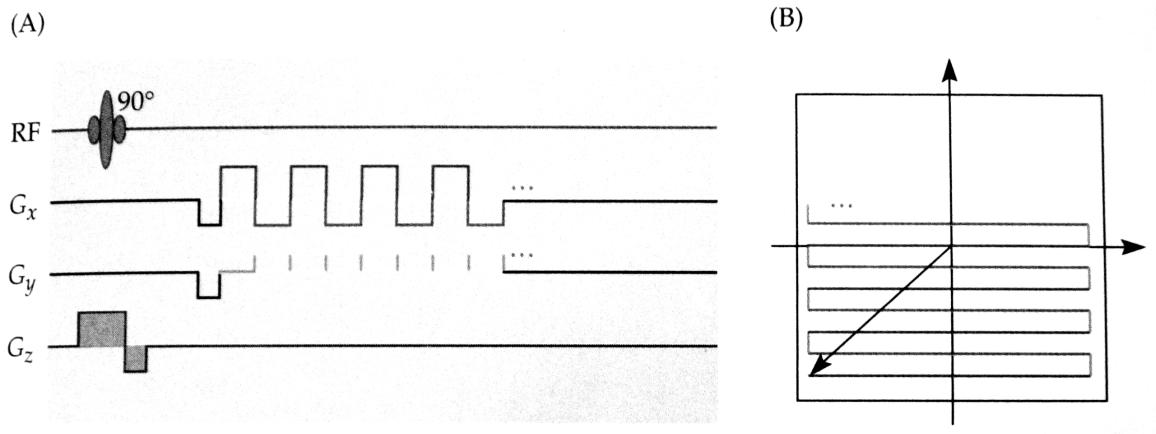

Figure 1-14.[9] (A) An EPI pulse sequence diagram and (B) a representation of its zig-zag trajectory in k-space.

In order to achieve contrast, all of k-space must be filled before substantial T2* decay has occurred, which is why this technology was limited until the early 1990s, when sufficiently powerful gradient systems had the capacity to rapidly switch on and off.[9]

In single-shot echo-planar imaging, the phase-encoding gradient is on continuously while the sign of the frequency encoding gradient inverts with each echo collected throughout a single TR. This pulse sequence allows k-space to be filled rapidly and continuously in a zig-zag pattern (Fig. 1-15). This form of acquisition is particularly taxing on the magnetic field gradients and raw data must be sorted and realigned to correct acquisition errors due to the zig-zag trajectory.[9] These technical issues were addressed with the advent of "blipped EPI," a method in which the phase encode gradient is applied in brief intervals, filling the same number of k-space lines in the same odd-even fashion without any required turnaround (Fig. 1-16a & b).[5] As a result, this method produces far fewer errors post-acquisition during Fourier transform.[5]

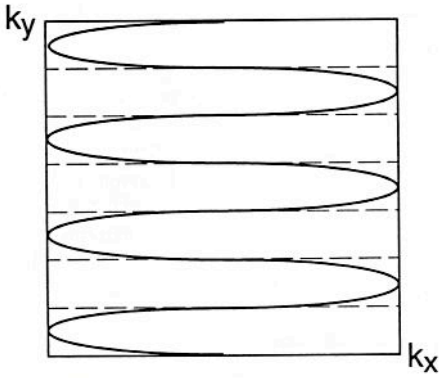

Figure 1-15.[5] Standard, single-shot EPI trajectory in k-space.

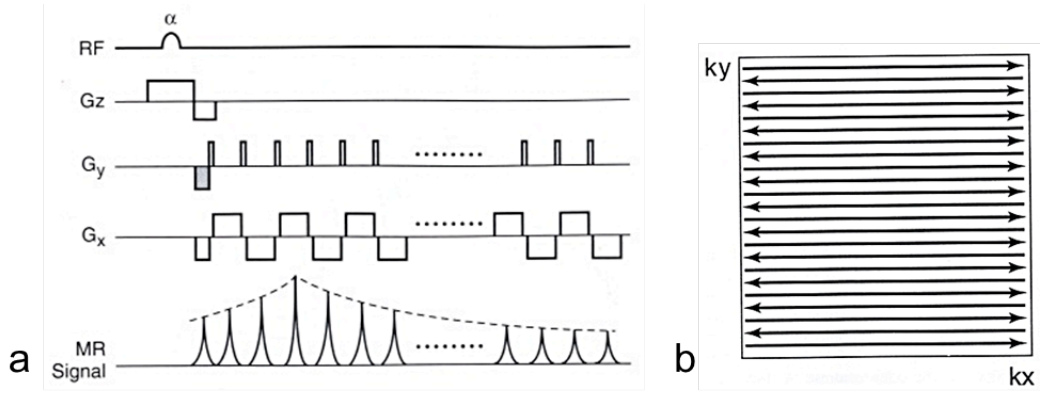

Figure 1-16.[5] Blipped EPI (a) pulse sequence diagram and (b) trajectory in k-space.

T2-weighted spin-echo pulse sequences are less commonly used in functional MRI due to their diminished sensitivity in comparison to T2*-weighted gradient-echo pulse sequences. However, because of the susceptibility artifacts that arise at brain-air interfaces in GE images, SE fMRI has grown in use, particularly in areas of songbird research.[11]

The most commonly used pulse sequence among advocates of SE fMRI is a fast spin echo (FSE) technique known as RARE (rapid acquisition with relaxation enhancement). RARE, like a conventional spin echo (CSE) pulse sequence, is characterized by an initial 90° RF pulse to flip proton spin magnetic moments into the transverse plane, followed by several 180° refocusing pulses, which serve to eliminate spin dephasing. Therefore, after each refocusing pulse, a new echo at maximum signal is collected at each TE (Fig. 1-17).

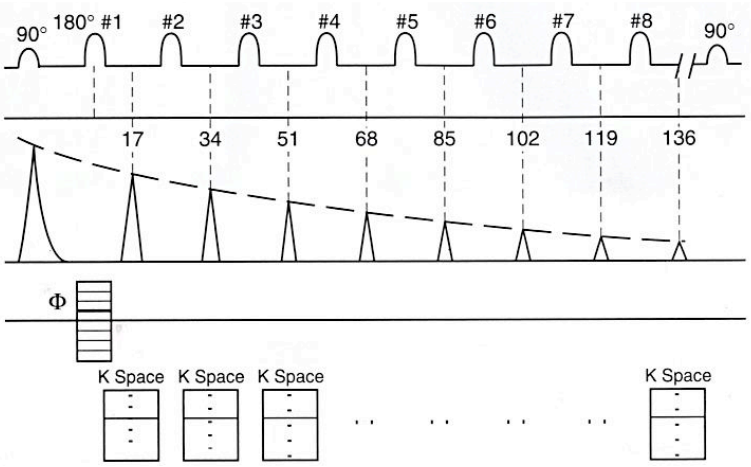

Figure 1-17.[5] In RARE image acquisitions, multiple refocusing pulses occur with within one TR. After each refocusing pulse, an echo is collected that fills several lines of k-space. This method allows us to acquire data at a far more rapid pace in comparison to CSE pulse sequences.

RARE has the ability to acquire an image more rapidly than CSE pulse sequences because it collects multiple echoes within each TR, and then fills k-space with all of the collected signals at once before repeating the process (Fig. 1-18). This strategy allows RARE to acquire images many times faster than a CSE method that would take an entire repetition time to record a single line of signal in k-space.

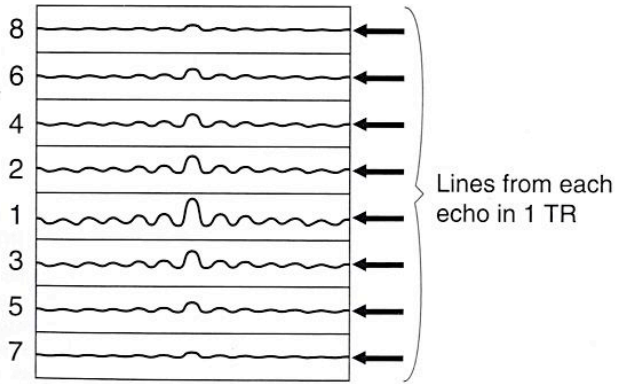

Figure 1-18.[5] FSE pulse sequences such as RARE fill multiple lines of k-space in a single TR.

Experimental Design and Post-processing

Functional imaging experiments aimed at determining the location of a neuronal response are best suited for a "block" experimental design.[12] In a block design (Fig. 1-19), the subject's neuronal response to the experimental stimulus is recorded during "task" or "on" periods. Meanwhile, during "rest" or "off" periods, functional images are acquired of the baseline BOLD signal.

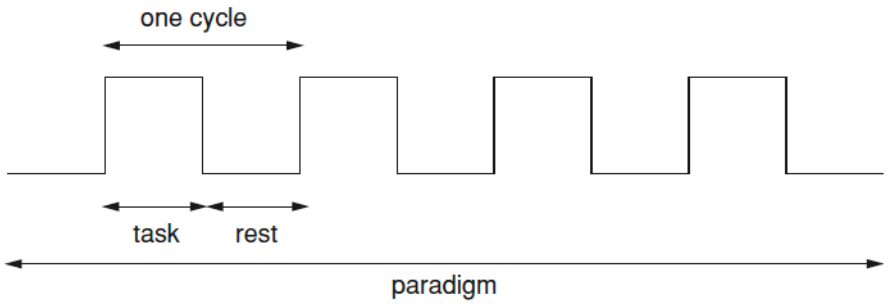

Figure 1-19[12]**.** A block paradigm for an fMRI experiment incorporates repeated cycles in which the neuronal response to a stimulus is measured during task periods, and baseline BOLD signal is measured during rest periods.

Timing is a very important factor to consider when designing an experimental paradigm. Since the BOLD response reaches its maximum approximately 5 seconds after stimulus onset, very short task periods should be avoided. Ideally, an experiment will incorporate "on" and "off" periods that are long enough for the BOLD response to reach a steady state.[12] Cycles involving 20-30 seconds of task and 20-30 seconds of rest are typical for most experiments.[12] Cycles are repeated to allow for statistical analysis during the post-processing stages. However, it is important to recognize that long experiment times increase the likelihood of motion artifacts due to discomfort, loss of concentration, and sensitization in some songbird studies.[12,13]

Once images are acquired according to an experimental paradigm, the basic concept of functional image processing is to subtract baseline signal associated with rest periods from signal associated with the cognitive task. However, there exist a number of processing and data analysis steps necessary to maximize signal, correct for errors in instrumental acquisition, and provide statistically relevant data. These pre-processing steps are usually implemented by a software package such as statistical parametric mapping (SPM) and commonly include the following:[12]

- Correction for common artifacts associated with echo-planar imaging such as distortion and signal dropout.
- Slice timing correction.
- Correction for motion artifacts.
- Global intensity normalization, which is implemented in areas of fluctuating BOLD signal.
- Spatial normalization, which is most often used when data from multiple subjects must be fit to a common template.
- Spatial and temporal smoothing with a Gaussian kernel improves SNR and also ensures that variance distribution is Gaussian.

Following pre-processing steps, statistical analysis is used to compile the entire collection of acquired images and determine which voxels have a significant probability of being associated with neuronal activation rather than noise. Statistical analysis is performed for each individual voxel to determine whether there is a non-zero probability that the volume element is part of the BOLD response.[12] Gaussian random field theory is commonly used among other methods of statistical analysis.[12]

One final important point to consider is that fMRI is a useful predictor of neuronal activity, but all fMRI data are considered correlational.[9] In other words, functional images can relate an event to a neuronal response, but they cannot establish a cause and effect relationship. For this reason, fMRI serves in many ways as a source of support for assertions made by other experimental methods that do implicate causation, such as electrophysiology.[9]

1.3 Songbird fMRI

Functional MRI is becoming an increasingly popular tool in the field of songbird research due to its ability to non-invasively provide whole-brain information relating to neural connectivity and function. This section will serve as an overview of the homologies motivating the study of songbird vocal learning, and introduce the technical challenges relevant to contemporary songbird imaging.

Established Human-Songbird Homologies

Numerous studies have indicated significant similarities between humans and songbirds on developmental, physiological and genetic levels. Such parallels are highly pertinent to experimental design, as well as to future studies on the songbird model and its relevance to neurological injuries and disorders. Thus, it is important to develop a solid understanding of these various homologies before proceeding discussions of vocal learning in this model organism.

Zebra finch vocal learning is developmentally and physiologically much like that of humans. Juveniles begin life in a sensitive period in which they are attuned to species-

specific sounds and learn from an adult male tutor. Non-singing females can also influence song learning in some cases. In zebra finches, song learning comprises two overlapping phases: First, in the memorization phase, the memory of the tutor song is acquired within a neural substrate referred to as a template. Second, in the sensorimotor phase, vocal output is matched to the memory of the tutor song in a trial and error process. As vocal output becomes more reproducible, the juvenile moves into a "plastic song" phase, which eventually produces the final product of song learning, a refined "crystallized song."[2]

It is a subject of debate whether a neural template for human language exists.[2] Nevertheless, it is significant that researchers have isolated a region in the zebra finch brain believed to be the neural substrate for the template for the memory of the bird's tutor song. The caudomedial nidopallium (NCM) (Fig. 1-20), thought to be the avian equivalent of Wernicke's area (Fig. 1-21), has been implicated in the memorization phase due to its role in auditory perception and auditory memory. As evidence, a 2012 study by Moorman et al. demonstrated that only in response to the tutor song would juvenile zebra finches show left-lateralized activation in the NCM.[14] Interestingly, this response is analogous to memory-specific, left-lateralized activation in Wernicke's area for speech perception in 2.5-month-old infants.[14]

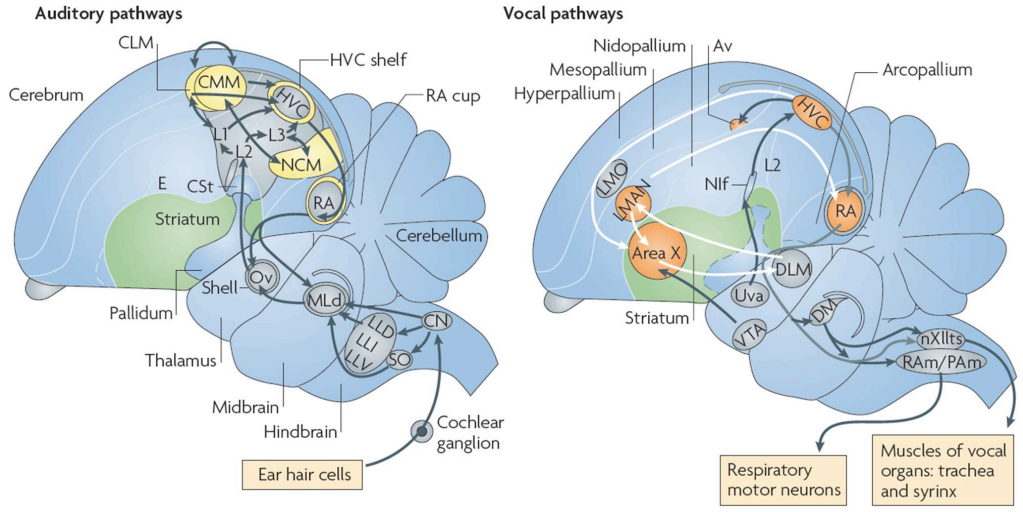

Figure 1-20.[2] Map of the songbird brain incorporating the auditory and vocal pathways, and their relevant structures.

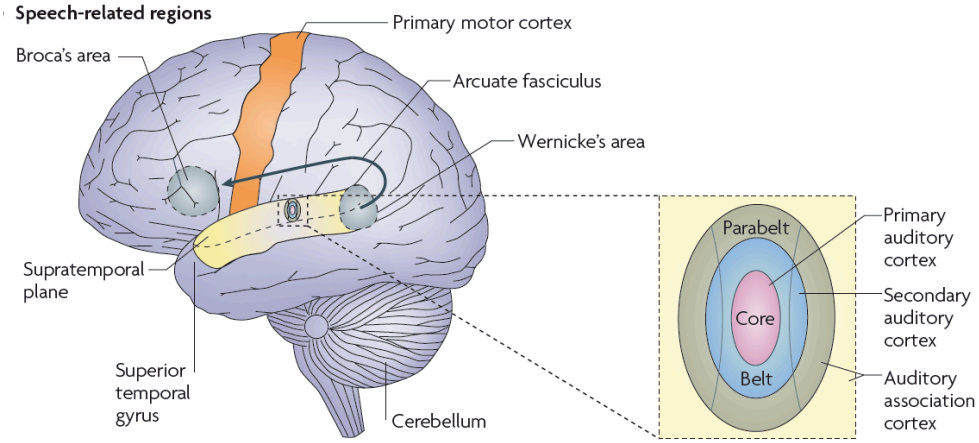

Figure 1-21.[2] Map of speech-related regions in the human brain.

Furthermore, these, among many studies, have demonstrated that songbirds, like humans, maintain a neural dissociation between vocal production and auditory memory and perception that is characterized by left-hemispherical dominance. For example, in response to conspecific song (tutor or unfamiliar), one study proved that adults and juveniles show left-hemispherical dominance of neuronal activation in the high vocal center (HVC) (Fig. 1-20), a region in the zebra finch brain analogous to Broca's area in

humans (Fig. 1-21).[14] Congruently, HVC plays a role in sensorimotor learning and song production.

By providing these parallels, such studies not only strengthen the songbird model for vocal learning but also lend support for the error correction model for the sensorimotor learning phase. A 2009 study by Poierer et al. suggests that both zebra finches and humans share a right-lateralized feedback control mechanism in the brain that monitors speech production and corrects for deviations from the expected auditory signal. In their study, Poirier et al. consistently found right-lateralized selectivity for bird's own song (BOS) in the HVC, Area X and lateral mesencephalic nucleus (MLd).[15] These results were demonstrated by significantly increased amplitudes of BOLD neural activation in response to BOS vs. conspecific song. Previous studies support the idea that BOS-selective brain regions participate in auditory feedback. Furthermore, similar findings in humans suggest that both zebra finches and humans evolved homologous physiology and mechanisms for auditory feedback.[15] Altogether, this provides strong evidence for HVC, Area X and MLd participation in this crucial learning process.

These few studies and many more comprise the large volume of human-bird physiological analogies, many of which correlate to developmental processes (Table 1-2, Fig. 1-20).

Human Brain	Songbird Brain
Neocortex	**Pallium (hyperpallium, mesopallium, nidopallium and arcopallium)**
Primary auditory cortex	**Field L**
Auditory association cortex (namely belt and parabelt regions)	**NCM and CMM**
Basal ganglia	**AFP loop in song system**
Broca's Area	**HVC**
Anterior Cingulate	**LMAN**

Table 1-2.[2] Researchers have identified a number of direct physiological homologies between the human brain and the songbird brain.

After the sequencing of the zebra finch genome, a number of genetic similarities between songbird and human vocalization were also discovered. Most notably, mutations in the transcription factor FOXP2 have been specifically linked with the speech disorder, developmental verbal dyspraxia, found in humans.[2] Likewise, when FOXP2 levels were experimentally reduced in zebra finches, juveniles could only partially copy the tutor song. Those elements of the tutor song that were copied were done so less accurately, and varied from rendition to rendition.[2] Altogether, FOXP2 knockdown's implications for song learning were highly similar to those for humans with DVD who are heterozygous for the FOXP2 mutation, and thus have difficulty producing complete and accurate word pronunciations.[2]

Technical Challenges

There are numerous practical challenges that confront the field of songbird fMRI due to the inherent nature of functional image acquisition and experimentation. The necessity to

immobilize the subject, produce the desired auditory stimulus, and acquire high-resolution, whole-brain data presents a wide range of difficulties that have been addressed in recent years. This section will address the most effective remedies to-date for the technical obstacles relevant to this field of study.

One of the greatest challenges affecting songbird fMRI is the prevalence of distortions and signal dropout in gradient-echo functional images. T2*-weighted GE pulse sequences are often favored in fMRI due to their heightened sensitivity, which results in a more substantial contrast-to-noise ratio (CNR).[11] Because SE pulse sequences are less sensitive to the BOLD response, they are far less prevalent in fMRI experiments at large. However, it is well established that GE pulse sequences produce susceptibility artifacts when used to image songbirds in fMRI experiments.[3,11]

Susceptibility artifacts consist of signal dropout and spatial distortions. These artifacts, which occur when magnetic field homogeneity cannot be established at brain-air interfaces, are exacerbated by GE imaging methods such as EPI, and high magnetic field strengths.[9] Because GE pulse sequences lack an 180° refocusing pulse, proton dephasing is not corrected, which results in more pronounced T2 and T2* decay.[5] This factor leads to a more pronounced loss of MR signal in GE images at brain-air interfaces, which are particularly abundant in songbirds. Spatial distortions in these images are attributable to the rapid gradient switching that characterizes echo planar imaging. This gradient switching EPI occurs due to the pulse sequence's zig-zag trajectory in k-space, as shown in Figures 1-15 and 1-16b. When such rapid changes occur in the orientation of the magnetic field gradients, there is an increased likelihood that an implementation error will occur that incorrectly modifies the magnetic field in the x, y or z direction over time. When such

an error occurs, the resultant variations in proton frequencies lead to a spatially distorted image.[5]

As a consequence of the prevalence of susceptibility artifacts in GE images, the majority of songbird fMRI experiments thus far have focused on the primary and secondary auditory regions, which are free of distortions and signal dropout.[11] While these studies have made valuable contributions to the field, it is clear that the use of GE pulse sequences imposes a substantial limitation on the study of the songbird brain. As a result, T1- and T2-weighted SE pulse sequences have been implemented in songbird fMRI.[3]

Most recently, the Bio-Imaging Laboratory at the University of Antwerp has proposed that T2-weighted SE fMRI produces more accurate whole-brain data than echo-planar imaging, with gradient noise levels that are more appropriate for auditory fMRI. In their 2010 study, Poirier et al. demonstrated that SE fMRI acquires signal in 99% of the avian brain, in comparison to less than 50% with GE sequences at 7T.[11] Furthermore, the RARE SE pulse sequence showed significant activation in MLd, a brain region known for its role in auditory feedback, in which GE pulse sequences have not been able to attain consistent signal due to signal dropout.[11] Poirier et al. also suggested that SE fMRI has better spatial specificity at high magnetic field strength. Because T2 relaxation time for venous blood is less than 10 ms at 9.4 T, the relatively long TE associated with SE pulse sequences allows for sufficient spin dephasing in large blood vessels, thereby removing their contribution to BOLD signal.[16] As a result, BOLD signal detected by a SE pulse sequence is of higher resolution and can be largely attributed to extravascular signal from the small capillaries responding to an increased metabolic demand.[11,16] This implies that

with stronger external magnetic fields, T2-weighted SE fMRI yields a weaker, yet more specific BOLD signal.

It is essential to immobilize animal subjects in order to avoid motion artifacts in imaging experiments. However, a point of controversy in small animal fMRI is whether sedation or anesthesia will produce productive or realistic experimental outcomes, since most experiments in humans are done with awake subjects. Yet, it is a significant challenge that conscious animal subjects often move, even when physically restrained. Training animals to tolerate the noisy MRI environment is very difficult and time-consuming, and variations in individuals' ability to focus on a listening task could mask the stimulus-specific BOLD response.[3] Although anesthesia does impact the BOLD response, previous studies on humans and birds have shown that the brain produces a meaningful response to auditory stimuli while the subject is asleep.[3,11] Because isoflurane is associated with the highest survival rate for birds with the fewest side effects and a relatively elevated BOLD response, it is often favored for functional imaging studies requiring repeated measurements.[11,17]

In functional imaging experiments, it is also vital to produce a very clear sound stimulus with minimal background noise. One issue with GE pulse sequences such as EPI is that they produce high amplitude, high frequency sounds due to gradient switching. These sounds could be difficult to discriminate from the auditory stimulus. The SE pulse sequence RARE produces lower frequency noise and is somewhat quieter, though still problematic. In their 2010 study, Poirier et al. lowered the amplitude of the gradient noise by increasing gradient ramp time to 600 μs, a common approach to this dilemma.[11]

Finally, there is the issue of maintaining a constant temperature inside the magnetic bore. Body temperature is known to have a significant impact on the hemodynamic response. In the 2010 study by Poirier et al., the group monitored body temperature and used feedback-controlled heating system to maintain the warm air being blown on the bird at a constant temperature.[11] Many other imaging systems incorporate a similar mechanism for this temperature-monitoring function.

Altogether, this project seeks to implement a comprehensive strategy for the functional magnetic resonance imaging of zebra finches for the study of vocal learning and memory. In doing so, it addresses the technical challenge of determining a suitable pulse sequence with appropriate scan parameters for rapid, artifact-free, high resolution, high signal to noise ratio functional imaging of a zebra finch subject. This study also attempts to resolve the practical issues relevant to sound delivery and subject motion throughout experimentation. This experimentation will culminate in the application of an auditory fMRI paradigm to examine the efficacy of the elected pulse sequence. Ultimately, these steps aim to achieve the overarching goal of establishing the protocol for an fMRI study of the neural processes underlying song development in the zebra finch.

2 Materials and Methods

2.1 Subjects and Subject Maintenance

Experiments were conducted on zebra finch, mouse and water-containing cylindrical phantom subjects.

All zebra finches were bred at the Wellesley College animal facility. The experimental group consisted of both male and female adult birds raised in isolation from singing males. Clutches of juveniles with their mothers were relocated to isolation coolers at 7 - 11 days post hatching (dph). Juveniles were moved to individual cages in separate coolers at 32 - 34 dph to prevent the siblings' exposure to each other's vocalizations. Control finches were raised with both parents. At 39 - 40 dph, each control bird was relocated to an individual cage in a separate isolation cooler. Preliminary experiments reported in the thesis did not involve an isolate-non-isolate comparison. These experiments made use of both male and female adult birds of all ages that were raised with both parents. All birds were identifiable by colored aluminum leg tags that were marked "WC" for Wellesley College followed by a number.

All subjects were on a 12 hour light/dark cycle and provided a constant supply of feed and water. Fresh bird feed was provided biweekly, and cages were cleaned once a week. Water was replenished as needed. Prior to each experiment, subjects were isolated from food for between 30 minutes and 1 hour to prevent choking during anesthetization.

The mouse used in a preliminary imaging experiment was a GCPII$^{(+/-)}$ heterozygous (HET) mouse descended from the founding colony at McLean hospital (Belmont, MA). This mouse contained a knockout of the GCPII gene and thus exhibited reduced GCPII enzyme function.[18] It was bred on campus at Wellesley College with procedures approved by the

Wellesley College Institutional Animal Care and Use Committee and that conform to the standards set forth in the National Institute of Health Guide for the Care and Use of Laboratory Animals.[18] The day after birth was considered postnatal day (PND) 1, and images were acquired on PND 55.

Wild type (WT) and HET mice in the Wellesley College animal facility, such as the one used in the experiment, were weaned on PND 21, on which day they were separated by sex into cages containing between two and four mice in total.[18] Like the birds, the mice were exposed to a 12 hour light/dark cycle and were provided with a constant supply of food and water. Systematic ear clippings identified mice in each cage. Ear samples were then used for genotyping at Mouse Genotype in Carlsbad, CA.

2.2 Magnetic Resonance Imaging

Brain MR images were acquired from male and female adult zebra finches (>80 dph) on a 9.4 T Bruker Avance 400 MHz vertical bore NMR spectrometer (2.4 G/cm/A gradient strength). Images were acquired using Bruker Paravision 4.0 software. Further image processing, including activation mapping and statistical analysis, was completed using Statistical Parametric Mapping (SPM) 8 software.

2.3 Subject Preparation

Zebra finches were anesthetized using 1.5-2% isoflurane in oxygen at a flow rate of 0.5 L/min in a plexiglass chamber (Braintree Scientific, Inc., Braintree, MA). Once anesthetized, the bird was transferred directly to a custom acrylic bed (Fig. 2-1). Anesthesia was directed into the nose cone of the bed such that the subject would remain

sedated. An exhaust tube located within the nose cone of the bed directed excess anesthesia into an external F/AIR Scavenger activated charcoal filter. The bird, positioned beak in nose cone, was secured in the acrylic bed using a layer of Kimtech Science Kimwipes® beneath 3M Micropore™ tape (Fig. 2-2). (The layer of Kimwipes® is intended to prevent the tape from damaging the bird's feathers.)

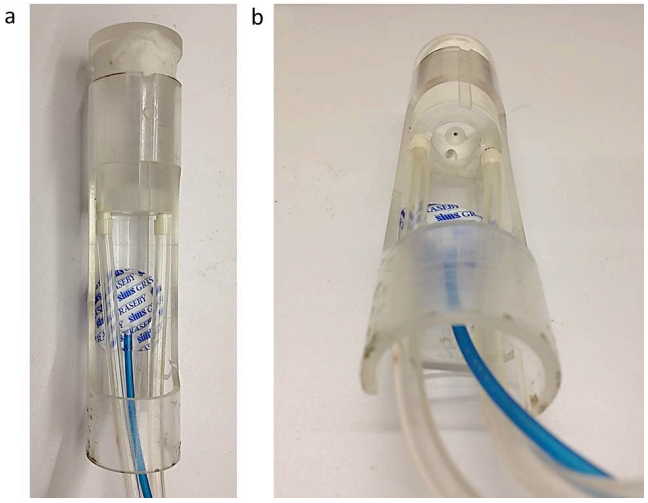

Figure 2-1. An acrylic bird bed was custom-made by Wellesley College mechanist Estuardo Rodas to accommodate a zebra finch in the micro-MRI probe. (a) An overhead view of the bed shows that it is equipped with two ports through which anesthesia is delivered and filtered out. (b) A side view shows the nose cone that allows the bed to accommodate the birds' beaks.

a

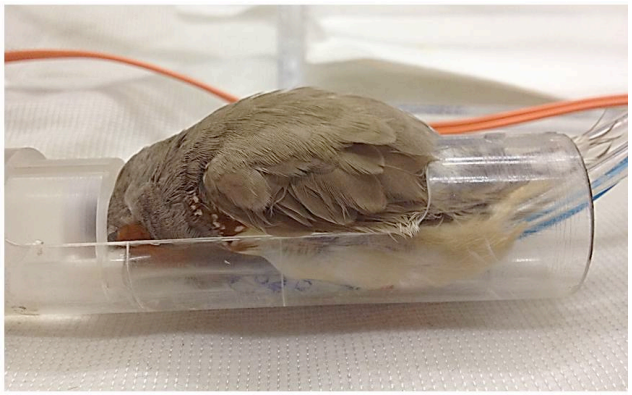

b

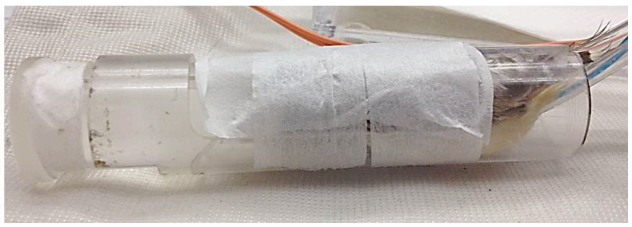

Figure 2-2. In preparation for imaging, (a) the subject is positioned with its beak into the nosecone of the acrylic bed to allow for optimal exposure to anesthesia. (b) The subject is then secured into the bed using a layer of Kimtech Science Kimwipes® beneath 3M Micropore™ tape.

Once taped into the acrylic bed, the bird's respirations were monitored visually and by using a pressure transducer pad compatible with BioTrig Builder 1.01 Software on a Dell Latitude laptop computer. The animal's respiration rate was regulated by adjusting isoflurane anesthesia levels with a VIP Veterinary Vaporizer. Respirations were maintained at levels between 50 and 100 breaths per minute. Once the animal had been safely anesthetized and secured in the acrylic bed, it was transferred into the MRI probe. Then the probe was inserted into the magnet such that the animal's brain aligned with the center of the gradient coils and RF coil. Throughout the experiment, a water circulation unit continually maintained a temperature of 35°C within the bore of the magnet to facilitate the subject's body temperature regulation.

2.4 Pulse Sequence Determination

The optimal pulse sequence for fMRI was determined by the comparison of two different imaging methodologies. Echo Planar Imaging (EPI), a gradient echo pulse sequence often used for fMRI, was applied to a cylindrical phantom, then to a mouse and a zebra finch. Subsequently, a RARE (rapid acquisition with relaxation enhancement) pulse sequence was used to image the zebra finch brain. For each pulse sequence, MRI parameters were experimentally adjusted to attain optimal image quality.

2.5 MRI Parameters

A predetermined shim file corresponding to the subject was loaded prior to each imaging session. All bird subjects were imaged according to a mouse shim due to the challenges of creating a homogeneous magnetic field over the air cavities in the songbird brain. Tuning and matching of the radiofrequency coils housed in the MRI probe preceded all image acquisitions. Following initial tuning and matching, each imaging session began with the use of a "RARE_tripilot" overview scan to confirm the proper positioning of the bird or mouse brain. "RARE_tripilot" scans were acquired in three orthogonal slices (Table 2-1). For all image acquisitions of animal subjects following the overview scan, fat suppression and motion suppression were applied to minimize signal from fat and reduce any motion artifacts due to physiological movement, respectively.

TR	TE	RARE Factor	Number of Averages	Matrix Size	Field of View (FOV)
2000.000 ms	**12.5 ms**	**8**	**1**	**128 x 128 pixels**	**2.56 x 2.56 cm^2**

Table 2-1. Parameters for overview scanning with a RARE_tripilot pulse sequence.

Anatomical Image Acquisition

All anatomical images were acquired using a "RARE_8_bas Params" T2 weighted pulse sequence (Table 2-2). 15 contiguous coronal slices (slice thickness = 0.75 mm; interslice distance = 0.75 mm) were acquired of the subject using "RARE_tripilot" images to position the field of view.

TR	TE	RARE Factor	Number of Averages	Matrix Size	Field of View (FOV)
3109.632 ms	**15 ms**	**8**	**8**	**256 x 256 pixels**	**2.56 x 2.56 cm^2**

Table 2-2. Parameters for anatomical image acquisition with a RARE_8_bas Prams pulse sequence.

EPI Trajectory Measurement with a Cylindrical Phantom

Gradient Echo (GE) images were acquired using an "EPI_bas" (echo planar imaging or "EPI") pulse sequence. Initially, a trajectory measurement was acquired of a cylindrical phantom containing water. Scan parameters are listed in Table 2-3 under Acquisition 1. An image was then acquired of a water-containing cylindrical phantom using the initially acquired trajectory measurement for reconstruction (Table 2-3, Acquisition 2). The scan protocol from this trajectory reconstruction was then saved with the name EPI_bas_64_agg.

Acquisition	1	2	3
Pulse Sequence	EPI_bas	EPI_bas (EPI_bas_64_agg)	EPI_bas
TR	2000.000 ms	2000.000 ms	2000.000 ms
TE	30 ms	30 ms	30 ms
Number of Averages	1	1	1
Matrix Size	64 x 64 pixels	64 x 64 pixels	64 x 64 pixels
Field of View (FOV)	2.0 x 2.0 cm^2	2.0 x 2.0 cm^2	2.0 x 2.0 cm^2
Slice Thickness	0.5 mm	0.5 mm	0.5 mm
Interslice Distance	0.5 mm	0.5 mm	0.5 mm
Trajectory Measurement	Yes	No	No
Use Trajectory For Reconstruction	No	Yes	No

Table 2-3. Parameters for echo planar image acquisition using an EPI_bas pulse sequence. A trajectory measurement was applied in Acquisition 1, followed by a trajectory reconstruction in Acquisition 2, whose scan protocol was later saved with the name "EPI_bas_64_agg." Acquisition 3 incorporated neither a trajectory measurement nor a trajectory reconstruction.

EPI Image Acquisition with a Mouse Subject

A Fastmap_8mm scan was applied at the start of the experiment to adjust first and second order shims over a 3 x 3 x 3 mm^3 cubic region. Eight contiguous images were acquired of a mouse brain using the "EPI_bas_64_agg" pulse program, which made use of the pre-programmed trajectory reconstruction described previously (Table 2-3, Acquisition 2). Echo planar imaging was also attempted using the pulse program "EPI_bas," for which the same pulse parameters were held constant, but a trajectory reconstruction was not used (Table 2-3, Acquisition 3).

EPI Image Acquisition with a Zebra Finch Subject

A Fastmap_8mm scan was applied at the start of the experiment to adjust first and second order shims over a 3 x 3 x 3 mm^3 cubic region. Twelve contiguous images were acquired of a zebra finch brain using the "EPI_bas_params" pulse program (Table 2-3, Acquisition 3). Both axial and sagittal views were acquired. In a follow-up zebra finch scan, the number of dummy scans was increased to 30 for the sagittal view. Echo planar imaging was also attempted with trajectory reconstruction using the pulse program "EPI_bas_64_agg" (Table 2-3, Acquisition 2).

RARE Image Acquisition with a Phantom Subject

Fast Spin Echo (FSE) images were acquired using a RARE (rapid acquisition with relaxation enhancement) pulse sequence. Experiments were conducted to produce maximum contrast to noise ratio with the minimum scan time. The effects of decreased TR, increased rare factor, decreased resolution (acquisition matrix) and decreased number of averages were considered. An initial experiment used a "RARE_8_bas" pulse program to demonstrate the effect of decreasing TR and the number of averages to a minimum (Table 2-4, Acquisitions 1 and 2). SNR was then calculated as the ratio of the mean signal intensity in a homogenous region of water to the mean signal intensity over air, exterior to the phantom. Signal intensity was determined using the Paravision ROI tool. SNR was calculated as the ratio of the mean signal intensity in a homogenous region of water to the mean signal intensity over air, exterior to the phantom.

Acquisition	1	2	3	4	5
Pulse Sequence	RARE_8_bas	RARE_8_bas	RARE_8_bas	RARE_8_bas	RARE_8_bas
TR	3109.632 ms	129.568 ms	2000.000 ms	2000.000 ms	2000.000 ms
TE	15 ms	15 ms	15 ms	15 ms	15 ms
RARE Factor	8	8	8	12	16
Number of Averages	8	1	1	1	1
Matrix Size	256 x 256 pixels	256 x 256 pixels	256 x 256 pixels	256 x 256 pixels	256 x 256 pixels
Field of View (FOV)	2.56 x 2.56 cm^2	2.56 x 2.56 cm^2	2.56 x 2.56 cm^2	2.56 x 2.56 cm^2	2.56 x 2.56 cm^2
Slice Thickness	0.5 mm	0.5 mm	0.75 mm	0.75 mm	0.75 mm
Interslice Distance	0.5 mm	0.5 mm	0.75 mm	0.75 mm	0.75 mm

Table 2-4. Parameters for RARE image acquisitions using a RARE_8_bas pulse sequence. Experiments aimed at testing the effects of TR, number of averages and RARE factor on scan time, resolution, SNR ratio and distortions.

In the following experiment, the "RARE_8_bas" pulse program RARE factor was increased from 8 to 12 to 16 while all other scan parameters were held constant (Table 2-4, Acquisitions 3, 4 and 5). SNR was then determined using the Paravision ROI tool with a 0.06 to 0.08 cm^2 circular region of interest. SNR was calculated as the ratio of the mean signal intensity in a homogenous region of water to the mean signal intensity over air, exterior to the phantom.

In a third experiment, matrix size was decreased from 64 x 64 pixels to 32 x 32 pixels using a "RARE_8_bas" pulse program. All other scan parameters were held constant (Table 2-5, Acquisitions 1 and 2). A third image acquisition showed the effect of changing the rare factor from 8 to 12 while matrix size = 32 x 32 pixels (rather than 64 x 64 pixels) and all other parameters are unchanged with respect to the previous acquisitions from the experiment (Table 2-5, Acquisition 3). SNR was then determined using the Paravision ROI tool with a 0.06 to 0.08 cm^2 circular region of interest. SNR was calculated as the ratio of the mean signal intensity in a homogenous region of water to the mean signal intensity over air, exterior to the phantom.

Acquisition	1	2	3
Pulse Sequence	RARE_8_bas	RARE_8_bas	RARE_8_bas
TR	2000.000 ms	2000.000 ms	2000.000 ms
TE	15 ms	15 ms	15 ms
RARE Factor	8	8	12
Number of Averages	1	1	1
Matrix Size	64 x 64 pixels	32 x 32 pixels	32 x 32 pixels
Field of View (FOV)	1.60 x 1.60 cm^2	1.60 x 1.60 cm^2	1.60 x 1.60 cm^2
Slice Thickness	0.75 mm	0.75 mm	0.75 mm
Interslice Distance	0.75 mm	0.75 mm	0.75 mm

Table 2-5. Parameters for RARE image acquisitions using a RARE_8_bas pulse sequence. Experiments aimed at testing the effects of matrix size and RARE factor on scan time, resolution, SNR ratio and distortions.

In a final experiment, two different reconstruction methods were assessed for their ability to produce a high-resolution, high SNR image while maintaining a short scan time. The first acquisition established a baseline for comparison, in which a 64 x 64 pixel matrix was applied without zero filling or a change in output or reconstruction (Table 2-6, Acquisition 1). The subsequent scan made use of an increased zero fill acceleration for an acquisition with a 64 x 64 pixel matrix size (Table 2-6, Acquisition 2). The final scan had a 32 x 32 pixel matrix size with an increased reconstruction size of 64 x 64 pixels and an

output size of 64 x 64 pixels to double the resolution of the resultant image (Table 2-6, Acquisition 3).

Acquisition	1	2	3
Pulse Sequence	RARE_8_bas	RARE_8_bas	RARE_8_bas
TR	2000.000 ms	2000.000 ms	2000.000 ms
TE	15 ms	15 ms	15 ms
RARE Factor	8	8	8
Number of Averages	1	1	1
Zero Fill Acceleration	1	2	1
Matrix Size	64 x 64 pixels	64 x 64 pixels	32 x 32 pixels
Acquisition Matrix	64 x 64 pixels	64 x 32 pixels	32 x 32 pixels
Output Size	64 x 64 pixels	64 x 64 pixels	64 x 64 pixels
Reconstruction Size	64 x 64 pixels	64 x 64 pixels	64 x 64 pixels
Field of View (FOV)	2.56 x 2.56 cm^2	2.56 x 2.56 cm^2	2.56 x 2.56 cm^2
Slice Thickness	0.75 mm	0.75 mm	0.75 mm
Interslice Distance	0.75 mm	0.75 mm	0.75 mm

Table 2-6. Parameters for RARE image acquisitions using a RARE_8_bas pulse sequence. Experiments aimed at testing the effects of zero filling, output size and reconstruction size on scan time, resolution, and SNR.

RARE Image Acquisition with a Zebra Finch Subject

Images were acquired using a "RARE_8_bas" pulse program. The number of averages was reduced from 8 to 4 to 2 to 1 average for a 32 x 32 acquisition matrix (Table 2-7). SNR was then determined using a 0.1 cm^2 circular region of interest in slice 7 of each image volume. SNR was calculated as the ratio of the mean signal intensity in a homogenous region of the right hemisphere to the mean signal intensity over air, outside the subject's body.

Acquisition	1	2	3	4
Pulse Sequence	RARE_8_bas	RARE_8_bas	RARE_8_bas	RARE_8_bas
TR	2000.000 ms	2000.000 ms	2000.000 ms	2000.000 ms
TE	15 ms	15 ms	15 ms	15 ms
RARE Factor	8	8	8	8
Number of Averages	8	4	2	1
Matrix Size	32 x 32 pixels	32 x 32 pixels	32 x 32 pixels	32 x 32 pixels
Field of View (FOV)	2.56 x 2.56 cm^2	2.56 x 2.56 cm^2	2.56 x 2.56 cm^2	2.56 x 2.56 cm^2
Slice Thickness	0.75 mm	0.75 mm	0.75 mm	0.75 mm
Interslice Distance	0.75 mm	0.75 mm	0.75 mm	0.75 mm

Table 2-7. Parameters for RARE image acquisitions using a RARE_8_bas pulse sequence. Experiments aimed at testing the effect of number of averages on scan time, resolution, SNR ratio and distortions.

In a second experiment, a RARE_8_bas pulse sequence was used to acquire two sets of images for which matrix size was 32 x 32 pixels, while output size and reconstruction size were doubled from 32 x 32 pixels to 64 x 64 pixels each. the effect of increasing output and reconstruction size on scan time, resolution and SNR were examined while keeping all other parameters constant. Scan parameters are listed in Table 2-8.

Acquisition	1	2
Pulse Sequence	RARE_8_bas	RARE_8_bas
TR	2000.000 ms	2000.000 ms
TE	15 ms	15 ms
RARE Factor	8	8
Number of Averages	1	1
Matrix Size	32 x 32 pixels	32 x 32 pixels
Output Size	32 x 32 pixels	64 x 64 pixels
Reconstruction Size	32 x 32 pixels	64 x 64 pixels
Field of View (FOV)	2.56 x 2.56 cm^2	2.56 x 2.56 cm^2
Slice Thickness	0.75 mm	0.75 mm
Interslice Distance	0.75 mm	0.75 mm

Table 2-8. Parameters for RARE image acquisitions using a RARE_8_bas pulse sequence. Experiments aimed at testing the effect of increasing output size and reconstruction size.

After acquiring images, SNR was determined using a 0.1 cm^2 circular region of interest in slice 7 of each image volume. SNR was calculated as the ratio of the mean signal intensity in a homogenous region of the right hemisphere to the mean signal intensity over air, outside the subject's body.

The effect of matrix size on scan time and image quality with a bird subject was examined. A "RARE_8_bas" pulse program was used to acquire images with matrix sizes 32 x 32 pixels and 64 x 32 pixels. Scan parameters are listed in Table 2-9.

Acquisition	1	2
Pulse Sequence	RARE_8_bas	RARE_8_bas
TR	2000.000 ms	2000.000 ms
TE	15 ms	15 ms
RARE Factor	8	8
Number of Averages	1	1
Matrix Size	32 x 32 pixels	64 x 32 pixels
Field of View (FOV)	2.56 x 2.56 cm^2	2.56 x 2.56 cm^2
Slice Thickness	0.75 mm	0.75 mm
Interslice Distance	0.75 mm	0.75 mm

Table 2-9. Parameters for RARE image acquisitions using a RARE_8_bas pulse sequence. Experiments aimed at testing the effect of matrix size on scan time, resolution, SNR ratio and distortions.

A "RARE-fMRI-TR2000" pulse program was used to examine whether a sound stimulus played on G-MAX 2000 Gateway external audio speakers would be capable of eliciting a BOLD response. A second goal of the experiment was to test the application of functional imaging data to Statistical Parametric Mapping (SPM) 8 software. Functional images were acquired during alternating 40 second periods of silence and song (Fig. 2-3) (Table 2-10). The subject was an adult male who had experienced normal song development. Periods of song began with 11 seconds of silence, followed by 3 seconds of random conspecific song alternating with 1 second of silence repeating over the course of 30 seconds. The initial silence during song periods occurred during the first 11 seconds of the 2 dummy scans preceding data acquisition. Each full block consisted of 2 dummy scans and 3 averaged data acquisitions as shown in Figure 2-4. The full paradigm consisted of 4 blocks of silence and 4 blocks of song, equally distributed among axial and sagittal image acquisitions. Images were subsequently processed in SPM8 according to the steps outlined in section 2.7 (Postprocessing).

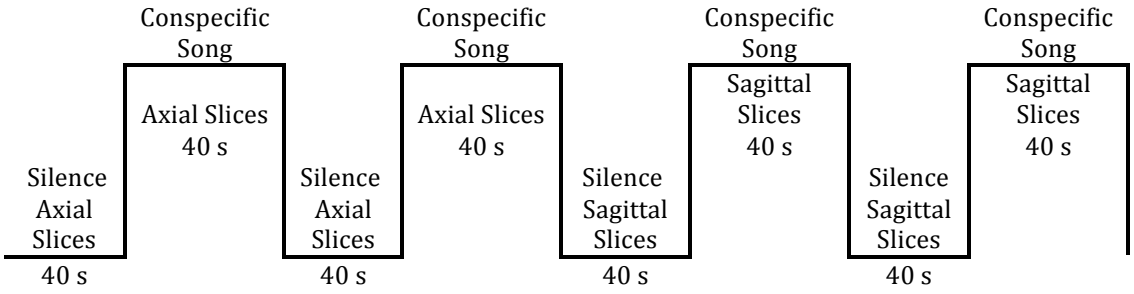

Figure 2-3. Functional images were acquired of the brain of an adult zebra finch that had undergone normal song development. The subject was subjected to four 40 second periods of silence alternating with four 40 second periods of exposure to random conspecific song. Acquisitions were evenly distributed among axial and sagittal slices.

Pulse Sequence	RARE-fMRI-TR2000
TR	2000.000 ms
TE	15 ms
RARE Factor	8
Number of Averages	3
Number of Dummy Scans	2
Matrix Size	64 x 32 pixels
Field of View (FOV)	2.56 x 2.56 cm^2
Output Size	64 x 32 pixels
Reconstruction Size	64 x 32 pixels
Number of Slices	15
Slice Thickness	0.75 mm
Interslice Distance	0.75 mm

Table 2-10. Parameters for RARE image acquisitions using RARE-fMRI-TR2000 and RARE_8_bas pulse sequences. Experiments aimed at testing the BOLD response in an adult male songbird exposed to conspecific song played by external speakers.

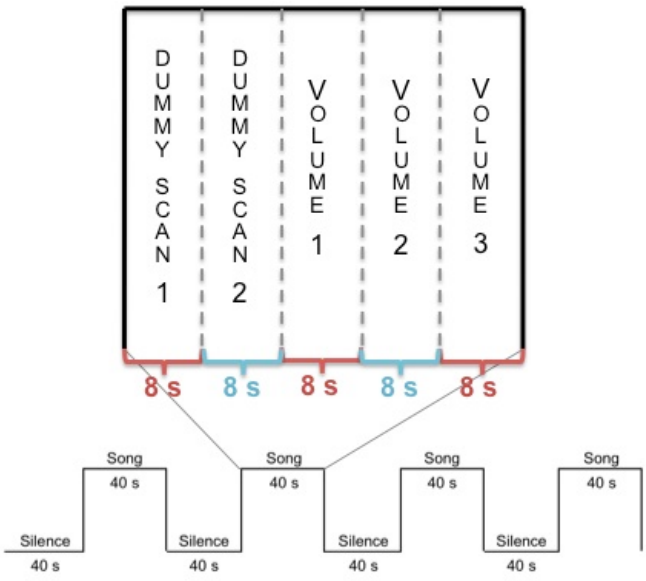

Figure 2-4. Blocks in the fMRI experiment consisted of two 8 second dummy scans followed by three 8 second data acquisitions, whole brain volumes of images that were subsequently averaged.

Next, in an effort to improve image quality, two different reconstruction methods were assessed for their ability to produce a high resolution, high SNR image while maintaining a short scan time and symmetrical pixels. Much like in the previous experiment with a phantom, "RARE_8_bas" images were acquired of an adult male zebra finch, first with a 32 x 32 pixel acquisition matrix, a 64 x 64 pixel output size and a 64 x 64 reconstruction size. Subsequently, images were acquired with a 64 x 64 acquisition matrix and a zero fill acceleration of 2. Full scan parameters are listed in Table 2-11 below.

Acquisition	1	2
Pulse Sequence	RARE_8_bas	RARE_8_bas
TR	2000.000 ms	2000.000 ms
TE	15 ms	15 ms
RARE Factor	8	8
Number of Averages	3	3
Zero Fill Acceleration	1	2
Matrix Size	32 x 32 pixels	64 x 64 pixels
Acquisition Matrix	32 x 32 pixels	64 x 32 pixels
Output Size	64 x 64 pixels	64 x 64 pixels
Reconstruction Size	64 x 64 pixels	64 x 64 pixels
Field of View (FOV)	1.40 x 1.40 cm^2	1.40 x 1.40 cm^2
Slice Thickness	0.75 mm	0.75 mm
Interslice Distance	0.75 mm	0.75 mm

Table 2-11. RARE_8_bas scan parameters for two different reconstruction methods. Experiments done on an adult male zebra finch aimed at establishing a protocol for the acquisition of high resolution, high SNR images with symmetrical pixels and a short scan time.

Then, a follow-up fMRI experiment applied a "RARE_8_bas" pulse program to re-test the G-MAX 2000 Gateway external audio speakers' capacity for eliciting a BOLD response and apply the resultant zebra finch data to SPM. The matrix size for this experiment was 32 x 32 pixels, with an output size of 64 x 64 pixels, a reconstruction size of 64 x 64 pixels, and a FOV of 1.40 x 1.40 cm^2 (Table 2-12). The subject was an adult male zebra finch who had experienced normal song development. Periods of song began with 11 seconds of silence, followed by 3 seconds of random conspecific song alternating with 1 second of silence repeating over the course of 30 seconds. The initial silence during song periods occurred during the first 11 seconds of the 2 dummy scans preceding data acquisition. Each full block consisted of 2 dummy scans and 3 averaged data acquisitions as shown in Figure 2-4. The full paradigm consisted of 4 blocks of silence and 4 blocks of song, consisting of all axial image acquisitions.

Pulse Sequence	RARE_8_bas
TR	2000.000 ms
TE	15 ms
RARE Factor	8
Number of Averages	3
Number of Dummy Scans	2
Matrix Size	32 x 32 pixels
Field of View (FOV)	1.40 x 1.40 cm^2
Output Size	64 x 64 pixels
Reconstruction Size	64 x 64 pixels
Number of Slices	15
Slice Thickness	0.75 mm
Interslice Distance	0.75 mm

Table 2-12. Parameters for RARE image acquisitions using RARE-fMRI-TR2000 and RARE_8_bas pulse sequences. Experiments aimed at testing the BOLD response in an adult male songbird exposed to conspecific song played by external speakers.

2.6 fMRI Paradigm

Sound stimuli were constructed from original recordings of adult male zebra finches made using 2011 SP1 (32-bit) 6-channel detect-record v2.0 software in conjunction with a SHURE 93 recording system attached to a NADY Audio PRA-8 8 channel mic pre-amplifier. Praat phonetics software was used to build a paradigm consisting of 40 second task periods and 40 second rest periods (Fig. 2-3). Task periods consisted of conspecific songs played to control birds (adults raised with a tutor) (Fig. 2-3). All rest periods consist of silence.

2.7 Postprocessing

Images were initially converted to .hdr/.img format using Analyze 11.0 software (AnalyzeDirect), and subsequently to NIfTI format using MRIcron software. The images could then be postprocessed using Statistical Parametric Mapping (SPM) 8 software.

Postprocessing began with image enlargement by a scale of 3, followed by the reorientation of the origin to a central location on the brain. Next, images were realigned such that each acquisition would be located in the same spatial position. Then, the set of images was coregistered to a template, an image of the subject's own anatomy from the experiment. Segmented images were also acquired, which consisted of the isolated white and gray matter from the brain. These images are utilized during Normalization and Rendering. Normalization followed, in which the template structural image is applied to the series of functional images. It is assumed that the structural image already fits the geometry of the functional images. Smoothing was then implemented to smooth image volumes with a Gaussian kernal full-width at half maximum (FWHM) of twice the voxel size. The specified model was for the paradigm shown in Figure 2-3, for which each block consisted of one acquisition with the parameters specified in Table 2-9. This model was applied to the acquired images to generate an activation map with the "overlays" function on SPM. See Appendix C: Guide to Postprocessing (Adapted from SPM8 Manual) for detailed instructions.

3 Results and Discussion

3.1 Pulse Sequence and Image Quality Assessment

An important prerequisite for experimentation is attaining optimal image quality. This section comprises an in-depth assessment of echo planar imaging (EPI) and Rapid Acquisition with Relaxation Enhancement (RARE) as candidates for functional imaging. Each pulse sequence's ability to produce effective functional images relies on both scan time and image quality. In order to capture the hemodynamic response, imaging must occur on the scale of seconds. Image quality is determined by each pulse sequence's resolution, signal-to-noise ratio (SNR) and predisposition towards susceptibility artifacts, which consist of signal dropout and spatial distortions.

EPI Image Acquisition with a Mouse Subject

Magnetic Resonance images of a mouse's brain (Fig. 3-1a) were acquired using the "EPI_bas_64_agg" pulse program, which applied a pre-programmed trajectory reconstruction. In that same imaging session, echo planar images were acquired of the subject's brain using the "EPI_bas" pulse program for which scan parameters were held constant, but a trajectory reconstruction was not used (Fig. 3-1b).

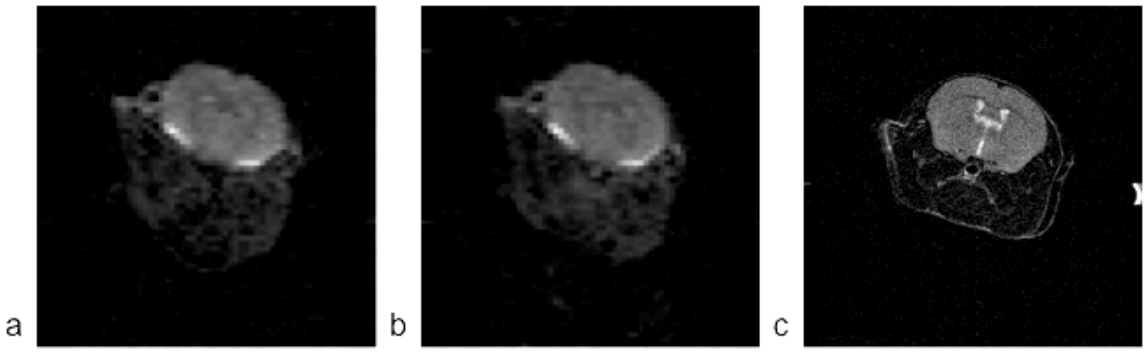

Figure 3-1. The quality of echo planar imaging of a mouse subject was assessed by the comparison of images acquired (a) with and (b) without a trajectory reconstruction. Further comparison was then made to (c) a high-resolution image acquired using a RARE pulse sequence.

No significant differences were observed between the two sets of images with and without trajectory reconstruction. Both sets of echo planar images were compared with a high-resolution structural image obtained during the same session (Fig. 3-1c). This comparison demonstrated that both echo planar imaging (EPI) pulse sequences maintained a relatively high level of fidelity to the shape and size of the subject's anatomy. However, there remained minor discrepancies in contrast and geometry between the sets of echo planar images and the more anatomically accurate RARE images. Resolution was lower because matrix size for the echo planar images was 64 x 64 pixels in comparison to 256 x 256 pixels for the Rapid Acquisition with Relaxation Enhancement (RARE) pulse sequence. The number of pixels in the phase encoding direction directly relate to the number of echoes collected in the pulse sequence, and the number of lines in k-space. Thus, because the EPI pulse sequence recorded fewer lines of k-space, it has both a lower resolution and a shorter acquisition time. As shown in Figure 3-1a & b, EPI images were acquired with a 64 x 64 pixel matrix size in 2.0 seconds, meanwhile Figure 3-1c is a RARE image acquired with a 256 x 256 matrix size in 5 minutes and 35.265 seconds.

These results make clear that although EPI is susceptible to geometric distortions and N/2 ghost artifacts, which are caused by gradient errors, our instrumentation does not appear to induce these artifacts.[5] Geometric distortions are typically caused by gradient nonlinearities or gradient power drop-off.[5] Meanwhile, N/2 ghost artifacts are typically the result of either eddy currents (small currents formed by rapid magnetic field gradient switching that can alter gradient implementation), imperfect gradients, magnetic field inhomogeneities or imperfect echo timing.[5] Additionally, while this pulse sequence has lower resolution than a standard RARE image, echo planar images can be acquired in the short amount of time required to capture the blood oxygen level dependent (BOLD) response.

However, it cannot be ignored that discrepancies in contrast and geometry, though small, did exist between the EPI and RARE images. Because trajectory reconstructions in Paravision correct gradient errors, any artifacts relevant to geometry and signal collection can most likely be classified as susceptibility-related effects. These susceptibility-related effects arise from magnetic field inhomogeneities.[19] The potential sources of such inhomogeneities in this case would be paramagnetic deoxyhemoglobin, fluid-filled ventricles and air-tissue interfaces in the subject. Since the geometry of the EPI images did not match the high-resolution structural images, it would be rather difficult to superimpose these two sets of images for functional image processing. Likewise, the discrepancies in contrast patterns between RARE and EPI bring into question whether the signal attained by EPI accurately reflected differences in the tissues. Because of this, EPI does not appear to be a promising candidate for functional imaging.

EPI Image Acquisition with a Zebra Finch Subject

MR images (Fig. 3-2a) were acquired of a zebra finch's brain using the "EPI_bas_params" pulse program. "EPI_bas_params" contained the same pulse programming as "EPI_bas," which was used in the previously described EPI experiment with a mouse subject. This new scan protocol differed from "EPI_bas" because its scan parameters (TR, TE, FOV, slice thickness and interslice distance) were pre-set. However, these pre-set values were identical to the ones used in the mouse experiment with "EPI_bas." In that same imaging session, echo planar imaging was also applied with a trajectory reconstruction using the pulse program "EPI_bas_64_agg," with the same pulse parameters as was used on a mouse in the previously described experiment (Fig. 3-2b).

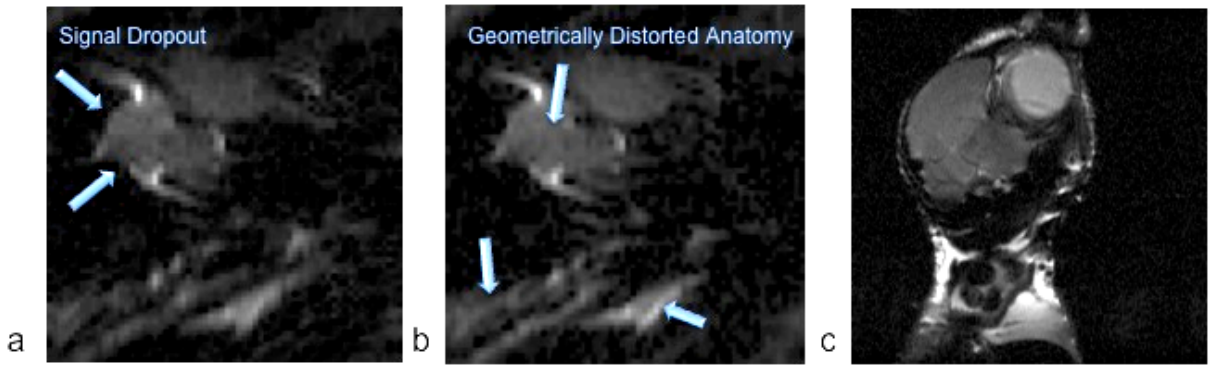

Figure 3-2. The quality of echo planar imaging of a zebra finch subject was assessed by the comparison of images acquired (a) with and (b) without a trajectory reconstruction. Further comparison was then made to (c) a high-resolution image acquired using a RARE pulse sequence.

Substantial geometrical distortions and signal dropout were observed in EPI images with and without trajectory reconstruction when compared to a high-resolution image acquired using a RARE pulse sequence (Fig. 3-2).

The absence of similar susceptibility artifacts in echo planar images acquired of the mouse subject (with and without trajectory reconstruction) strongly suggests that the

source of these artifacts is not instrumental, but attributable to the air cavities in the bird's skull. Previous studies have established a relationship between susceptibility artifacts (signal dropout and spatial distortions) and gradient echo (GE) pulse sequences such as EPI.[3,11] These artifacts, which occur when magnetic field homogeneity cannot be established at brain-air interfaces, are exacerbated by fast imaging methods and high magnetic field strengths.[9] This is because GE pulse sequences lack an 180° refocusing pulse.[5] As a result, proton dephasing is not corrected, which results in increased T2 and T2* decay. This problem is intensified at high magnetic field strengths. Ultimately, these factors lead to loss of MR signal in GE images at brain-air interfaces, which are abundant in songbirds. Spatial distortions in these images are attributable to the rapid gradient switching that characterizes echo planar imaging. This gradient switching EPI occurs due to the pulse sequence's zig-zag trajectory in k-space, as shown in Figure 3-3. When such rapid changes occur in the orientation of the magnetic field gradients, there is an increased likelihood that an implementation error will occur that incorrectly modifies the magnetic field in the x, y or z direction over time. When such an error occurs, the resultant variations in proton frequencies lead to a spatially distorted image.[5]

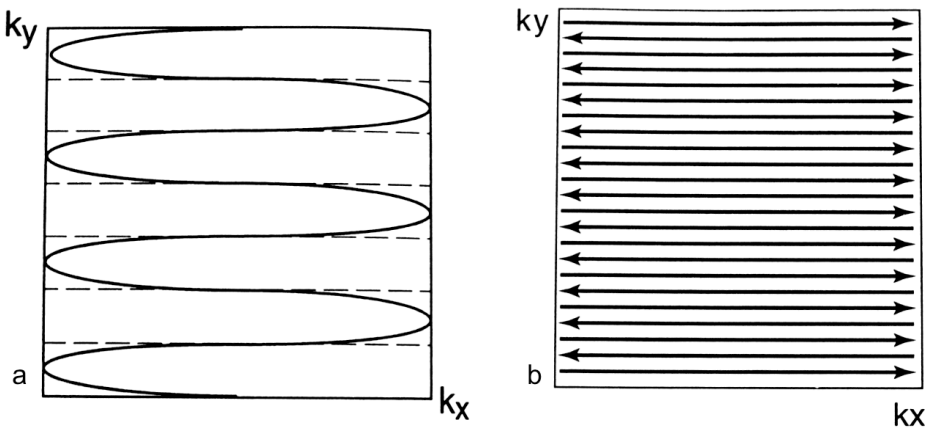

Figure 3-3. K-space trajectory for a (a) single shot and (b) multi-shot EPI pulse sequence.[5]

In conclusion, it is logical that susceptibility artifacts would appear in echo planar images of songbirds, whose skulls contain substantial air cavities. Meanwhile, mice contain minimal brain-air interfaces, and therefore are less susceptible to this form of artifact. Thus, we introduced another pulse sequence to determine its capacity for rapid, high-quality functional imaging.

RARE Image Acquisition with a Phantom Subject

The following experiments determined the effects of repetition time (TR), RARE factor and matrix size on image quality and acquisition time using a "RARE_8_bas" pulse program. TR is defined as the time after which an RF pulse is reapplied in an imaging experiment. RARE factor refers to the number of echoes collected within each TR and matrix size is the parameter the directly correlates to the image's in-plane resolution in pixels. The subject for each experiment was a water-containing cylindrical phantom. In the first experiment, all other scan parameters were held constant while images were acquired with a typical TR

of 3109.632 ms and with a minimized TR of 120.568 ms. Number of averages was also reduced from a 8 to 1 in this experiment.

The reduction in TR and number of averages resulted in a scan time of only 3.86 seconds, but extremely poor image quality (Fig. 3-4b, Table 3-1). Table 3-1 demonstrates that when TR and number of averages significantly decrease, signal-to-noise (SNR) ratio decreases to nearly 1. The cylindrical phantom was not discernable from the background, suggesting that the TR was not long enough to apply a sufficient number of refocusing pulses and collect enough echoes to fill the 256 lines of k-space required for a 256 x 256 matrix size.

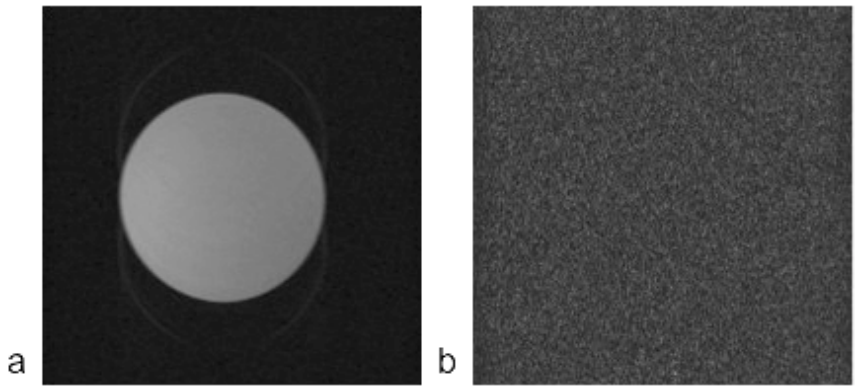

Figure 3-4. A cylindrical phantom was imaged using a "RARE_8_bas" pulse program with (a) a TR of 3109.632 ms and 8 averages, and (b) a TR of 120.568 ms and 1 average.

TR	Number of Averages	Scan Time	SNR
3109.632 ms	**8**	**13 min 16.65 s**	**35.43**
129.568 ms	**1**	**0 min 3.86 s**	**1.03**

Table 3-1. Images of a cylindrical phantom were acquired using a "RARE_8_bas" pulse sequence. TR was decreased from 2000 ms to a minimum value of 129.568 ms and the number of averages was decreased from 8 to a minimum value of 1 while all other parameters were held constant to demonstrate the effect on scan time and image quality.

In a second experiment, RARE factor was increased from 8 to 12 to 16 while all other scan parameters were held constant. The data obtained from these trials showed that for this set of scan parameters, scan time could be significantly decreased when RARE factor is increased from 8 to 12 (Table 3-2). However, any further increase in RARE factor does not affect scan time (Table 3-2). Furthermore, each increase in RARE factor resulted in a significant decrease in SNR (Table 3-2, Fig. 3-6).

Upon further inspection, it became evident that although scan time decreased as RARE factor was increased from 8 to 12, increasing RARE factor also lead to a subsequent increase in TR (Table 3-2, Fig. 3-5). The explanation as to why scan time initially decreased while TR increased is that RARE factor refers to the number of 180° refocusing pulses implemented and the number of echoes subsequently collected within a given TR. As a result, although TR has increased, the number echoes collected in each TR has also increased. Each echo translates to a line of data in k-space, and k-space is filled more quickly as a result of increased RARE factor.

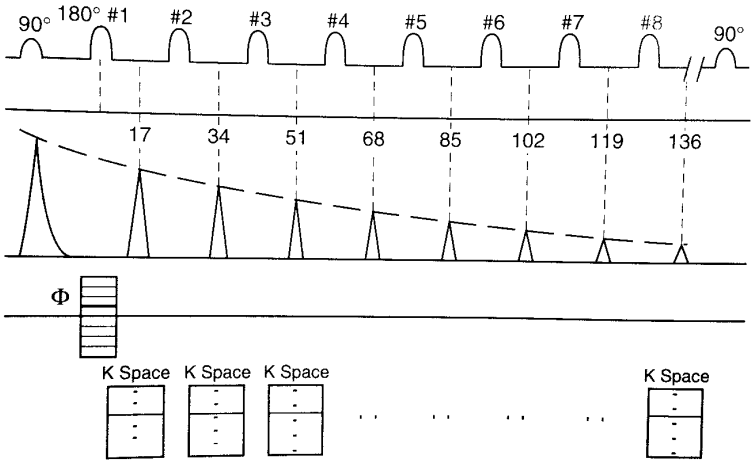

Figure 3-5. A key feature of RARE pulse sequences is the implementation of multiple 180° refocusing pulses and subsequent echoes that are collected.[5]

RARE Factor	TR	TE	Effective TE	Scan Time	SNR
8	2000.000 ms	15 ms	60 ms	64.000 s	5.02
12	2843.520 ms	15 ms	90 ms	59.713 s	4.05
16	3743.520 ms	15 ms	120 ms	59.896 s	3.17

Table 3-2. The effect of changing RARE factor on scan time for a FSE "RARE_8_bas" pulse program.

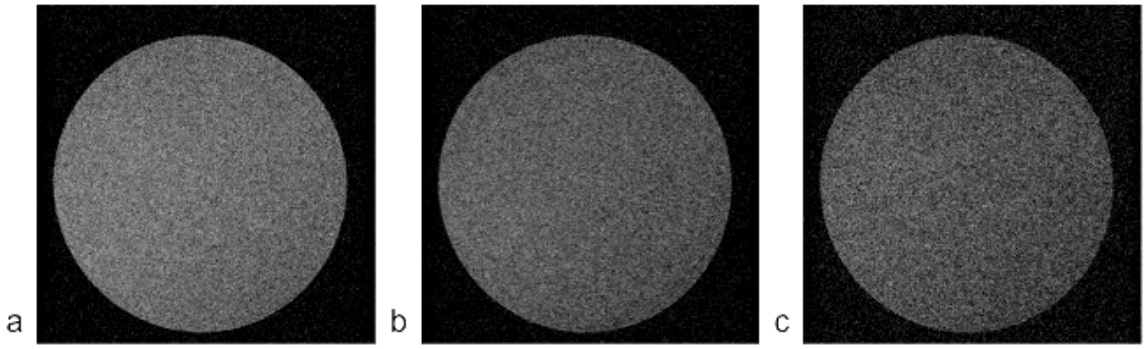

Figure 3-6. Images of a cylindrical phantom were acquired using a RARE pulse program for which RARE factor was increased from (a) 8 to (b) 12 to (c) 16 and all other scan parameters were held constant.

A third experiment examined the effect of decreasing acquisition matrix size from 64 x 64 pixels to 32 x 32 pixels (minimum matrix size) while all other scan parameters were held constant. Results are summarized in Table 3-3. When matrix size was reduced by a factor of 2, scan time decreased by a factor of 2. This is because the number of pixels in the phase encoding direction, designated by the second dimension of the acquisition matrix size, directly correlates to the number of lines of k-space required to form an MR image. Thus, recording half as many lines in k-space requires half the scan time.

Furthermore, while decreased matrix size had a clear effect on resolution, producing noticeably larger pixels, it actually increased SNR and did not add any distortions (Table 3-3, Fig. 3-7). In this initial experiment, RARE factor was also increased from 8 to 12 for an acquisition matrix size of 32 x 32 pixels and otherwise unchanged scan parameters. Scan

time was reduced from 8 seconds to 5.6 seconds when RARE factor was changed from 8 to 12 (Table 3-3). As explained previously, the reason for this is because k-space could be filled in fewer repetition times due to the increased number of echoes collected in each TR. However, SNR underwent a moderate decrease from 40.07 to 33.72 (Table 3-3). This makes sense, because TR is increased, meanwhile TE remains constant. This allows for more longitudinal relaxation of the nuclear magnetic moments in the sample. This leads to a decrease in T1 weightedness, more pronounced T2 weightedness and an overall decrease in signal for the image (Fig. 3-8). The result is the decreased SNR as shown in Table 3-3.

RARE Factor	Matrix Size	TR	TE	Effective TE	Scan Time	SNR
8	64 x 64 pixels	2000.000 ms	15.000 ms	60.00 ms	16.000 s	24.16
8	32 x 32 pixels	2000.000 ms	15.000 ms	60.00 ms	8.000 s	40.07
12	32 x 32 pixels	2809.995 ms	15.000 ms	105.00 ms	5.619 s	33.72

Table 3-3. Images of a cylindrical phantom were acquired using a "RARE_8_bas" pulse sequence. Matrix size and RARE factor were systematically changed to demonstrate these parameters' effects on scan time and image quality.

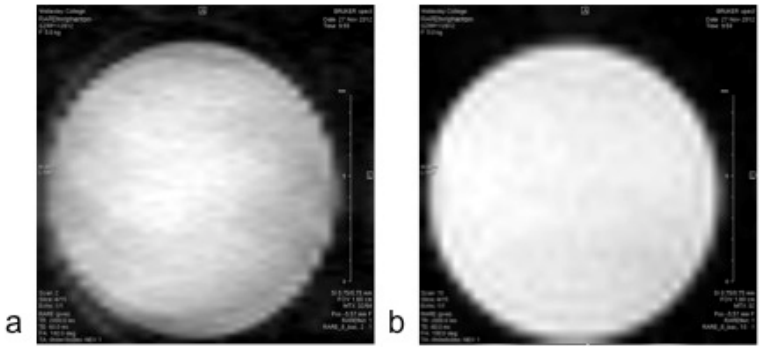

Figure 3-7. "RARE_8_bas" images were acquired of a cylindrical phantom with (a) a matrix size of 64 x 64 pixels and (b) a matrix size of 32 x 32 pixels. All other scan parameters were held constant.

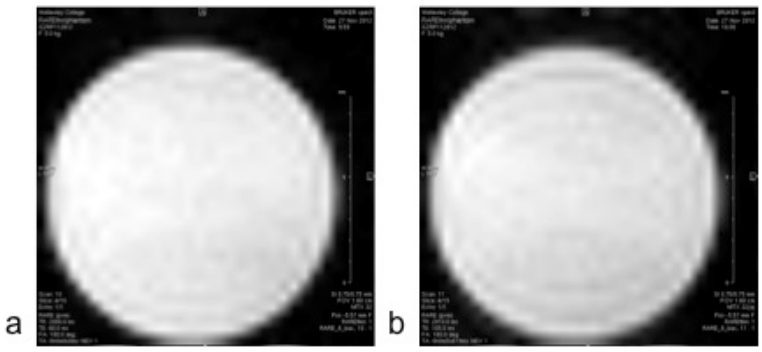

Figure 3-8. "RARE_8_bas" images were acquired of a cylindrical phantom with (a) a RARE factor of 8 and (b) a RARE factor of 12. All other scan parameters were held constant.

A final experiment was conducted to establish the efficacy of two different reconstruction methods for producing images with high resolution and high SNR within minimal scan time. An initial control scan was acquired with a 64 x 64 pixel matrix size, without zero filling, and without any alterations to output size or reconstruction size (Table 3-4, Fig. 3-9). The second scan was acquired with a zero fill acceleration of 2 and all other scan parameters held constant (Table 3-4, Fig. 3-9). The third acquisition had a matrix size of 32 x 32 pixels, an output size of 64 x 64 pixels, and a reconstruction size of 64 x 64 pixels (Table 3-4, Fig. 3-9).

Acquisition	1	2	3
TR	2000.000 ms	2000.000 ms	2000.000 ms
TE	15 ms	15 ms	15 ms
Zero Fill Acceleration	1	2	1
Matrix Size	64 x 64 pixels	64 x 64 pixels	32 x 32 pixels
Acquisition Matrix	64 x 64 pixels	64 x 32 pixels	32 x 32 pixels
Output Size	64 x 64 pixels	64 x 64 pixels	64 x 64 pixels
Reconstruction Size	64 x 64 pixels	64 x 64 pixels	64 x 64 pixels
Field of View (FOV)	2.56 x 2.56 cm^2	2.56 x 2.56 cm^2	2.56 x 2.56 cm^2
Scan Time	16.000 s	8.000 s	8.000 s
SNR	47.05	61.13	87.23

Table 3-4. Images of a water-containing cylindrical phantom were acquired using a "RARE_8_bas" pulse sequence. Experiments aimed at testing the effects of zero filling, output size and reconstruction size on scan time, resolution and signal to noise ratio.

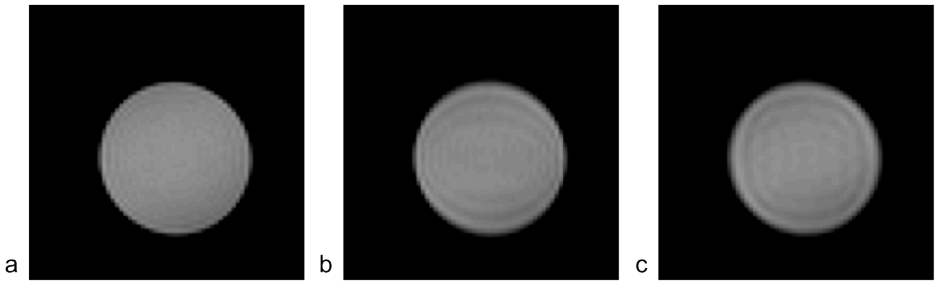

Figure 3-9. "RARE_8_bas" images were acquired of a cylindrical phantom with (a) no change in zero fill acceleration, output size or reconstruction size, (b) a zero fill acceleration of 2 and (c) no zero fill acceleration, and matrix size decreased by a factor of 2 with respect to output size and reconstruction size.

Both experimental acquisitions had half the scan time of the control acquisition and higher signal to noise ratios in comparison (Table 3-4). These results make sense because the key feature of zero filling is a rectangular acquisition matrix that is symmetrically "filled" with zeroes at the edge of k space, which correspond to high spatial frequencies but do not contain real signal information.[5] The addition of these "zeroes" allows the system to form a square matrix before Fourier-transform, and artificially decrease pixel size to

achieve higher resolution.[8] Thus, upon image acquisition, there is more signal collected per pixel in the 64 x 32 pixel acquisition matrix in comparison to a conventional 64 x 64 pixel acquisition matrix with the same field of view. The end result is that the zero-filled image collects more signal per pixel, and therefore has a higher SNR than an image of the same resolution without zero filling. Additionally, because fewer lines of data are recorded in k-space for a 64 x 32 pixel acquisition matrix, scan time is decreased.

The image collected with a 32 x 32 pixel acquisition matrix must have an even higher SNR because its acquisition matrix contains even larger pixels containing more signal than those in the zero-filled image with the same field of view. Scan time is identical to that of the zero-filled image because both scans have the same resolution in the spatial domain, and therefore record the same number of lines of k-space per acquisition. This scan is able to artificially maintain a resolution equal to that of the previous scans because its output and reconstruction sizes are increased with respect to the size of the acquisition matrix. Altogether, because this third method of acquisition could acquire images of minimum scan time, equal resolution and improved SNR with respect to the other scans, it was favored for future fMRI experiments using zebra finches (Table 3-4).

RARE Image Acquisition with a Zebra Finch Subject

The following experiments assessed the effect of averages, matrix size, and RARE factor on acquisition time and overall image quality. Subjects were anesthetized adult zebra finches. In the first experiment, images were acquired when the number of averages was reduced from 8 to 4 to 2 to 1 (Fig. 3-10a-d). All other scan parameters were held constant. Theoretically, an instrument's signal-to-noise ratio should increase with the square root of

the number of averages. However, with the use of the Paravision ROI tool, it was determined that SNR was lower than expected, which is logical, since a simple calculation does not account for other sources of noise such as thermal noise generated by the vibrating gradients (Fig. 3-10, Table 3-5). Furthermore, scan time decreased linearly with the number of averages (Table 3-5). This makes sense mathematically because each scan is identical to all other scans in the set that is being averaged.

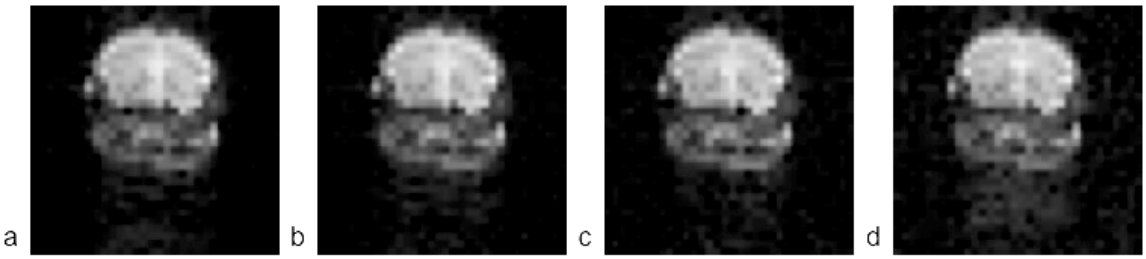

Figure 3-10. "RARE_8_bas" images of a live zebra finch were acquired with (a) 8 averages, (b) 4 averages, (c) 2 averages, and (d) 1 average. All other scan parameters were held constant.

Acquisition	Number of Averages	Scan Time	SNR	Expected SNR
1	8	64.000 s	45.82	63.3
2	4	32.000 s	39.09	44.76
3	2	16.000 s	24.21	31.65
4	1	8.000 s	22.38	22.38

Table 3-5. Images of a live zebra finch were acquired using a "RARE_8_bas" pulse sequence. The number of averages was systematically decreased to demonstrate this parameter's effect on scan time and image quality.

A second experiment reexamined the effect of matrix size on scan time and image quality. A "RARE_8_bas" pulse sequence was used to acquire images of the zebra finch subject with an acquisition matrix size of 32 x 32 pixels. The first set of images was acquired with a 32 x 32 reconstruction size and a 32 x 32 output size (Fig. 3-11a). The second image was acquired with a 64 x 64 reconstruction size and a 64 x 64 output size.

The resultant images had a noticeably smaller pixel size (Fig. 3-11b) and thus better resolution. Pixel size for the second set of images was 0.4 x 0.4 mm^2, indicating that our parameter changes effectively increased the in-plane resolution while maintaining a fast scan time (Table 3-6). Additionally, this increase in resolution resulted in only a slight loss in SNR (Table 3-6).

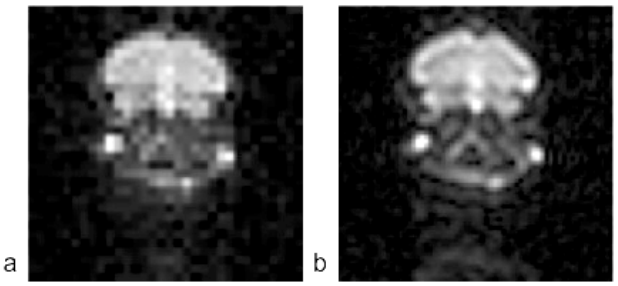

Figure 3-11. Images of a zebra finch were acquired using a "RARE_8_bas" pulse sequence. Resolution in the time domain was adjusted by changing matrix size from (a) 32 x 32 pixels to (b) 32 x 32 pixels with an output size of 64 x 64 pixels and a reconstruction size of 64 x 64 pixels.

Acquisition	1	2
TR	2000.000 ms	2000.000 ms
TE	15 ms	15 ms
RARE Factor	8	8
Number of Averages	1	1
Matrix Size	32 x 32 pixels	32 x 32 pixels
Output Size	32 x 32 pixels	64 x 64 pixels
Reconstruction Size	32 x 32 pixels	64 x 64 pixels
Scan Time	8.000 s	8.000 s
Pixel Size	0.8 x 0.8 mm^2	0.4 x 0.4 mm^2
SNR	22.375	20.27

Table 3-6. Parameters are displayed from two sets of images acquired using a "RARE_8_bas" pulse sequence. The subject was an adult zebra finch.

Functional MRI experiments were conducted to examine the G-MAX 2000 Gateway external audio speakers' capacity for eliciting a BOLD response and apply the resultant

zebra finch data to SPM. The first experiment in the series of two acquired images in alternating blocks of silence and song with a 64 x 32 pixel matrix size. Due to this asymmetrical acquisition matrix, pixels from the first experiment were rectangular, 0.4 x 0.8 mm^2 in size, and the images were misshapen (Fig. 3-12a). The resultant axial images, two volumes acquired in silence and two volumes acquired with a conspecific song stimulus, were processed in SPM.

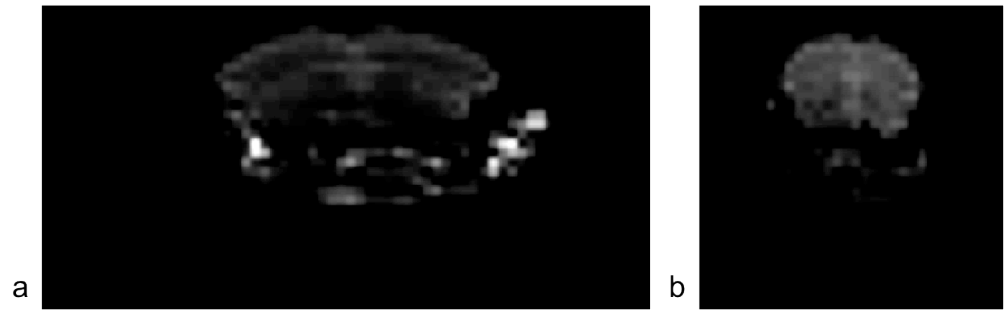

Figure 3-12. MR images acquired in an fMRI experiment with (a) an asymmetric 64 x 32 pixel matrix size and (b) a 32 x32 pixel matrix size displayed for comparison.

During initial processing with SPM 8, images were centered and increased in size by a factor of three. Processing steps produced result maps with a maximum intensity projection indicating the presence of BOLD contrast (Fig. 3-13).

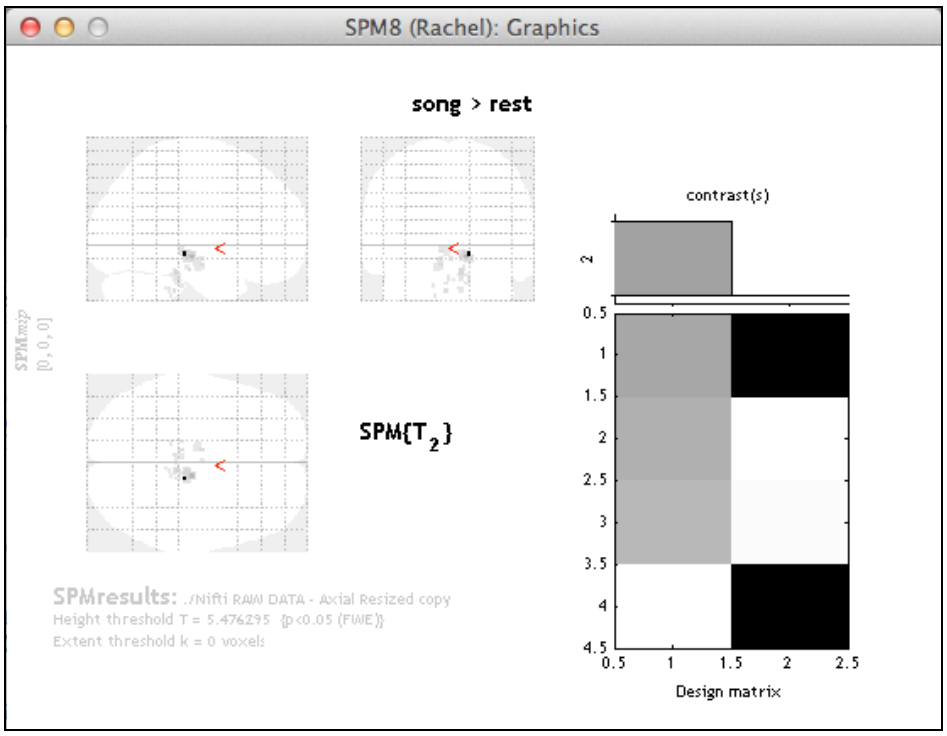

Figure 3-13. Maximum Intensity Projection of a statistical activation map representing the auditory BOLD response "song > rest" for a zebra finch subject.

However, the resultant 2D (Fig. 3-14a) and 3D (Fig. 3-14b) overlay maps indicated that imaging data was spatially misinterpreted. This is most likely attributable to the fact that SPM software and its instruction manuals are designed for the analysis of human MR images. Further investigation should be aimed at adjusting SPM 8 parameters for use with zebra finch data sets.

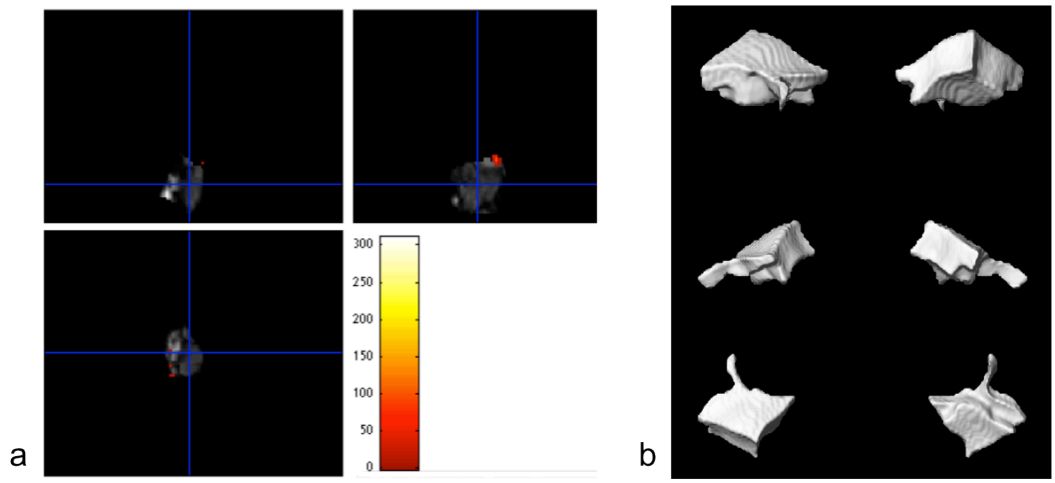

Figure 3-14. (a) 2D and (b) 3D overlay maps representing zebra finch whole-brain fMRI data processed using SPM 8.

A follow-up experiment was conducted to examine the efficacy of two different reconstruction methods for functional imaging. Both sets of images were assessed on the basis of their ability to produce high resolution, high SNR images in a short period of time and with symmetrical pixels. The first acquisition had a matrix size of 32 x 32 pixels, an output size of 64 x 64 pixels, and a reconstruction size of 64 x 64 pixels (Table 3-6 Acquisition 1, Fig. 3-15). The second scan was acquired with a zero fill acceleration of 2, an acquisition matrix of 64 x 32 pixels, an output size of 64 x 64 pixels and a reconstruction size of 64 x 64 pixels (Table 3-6 Acquisition 2, Fig. 3-15).

Acquisition	1	2
Pulse Sequence	RARE_8_bas	RARE_8_bas
TR	2000.000 ms	2000.000 ms
TE	15 ms	15 ms
Zero Fill Acceleration	1	2
Matrix Size	32 x 32 pixels	64 x 64 pixels
Acquisition Matrix	32 x 32 pixels	64 x 32 pixels
Output Size	64 x 64 pixels	64 x 64 pixels
Reconstruction Size	64 x 64 pixels	64 x 64 pixels
Field of View (FOV)	1.40 x 1.40 cm^2	1.40 x 1.40 cm^2
Pixel Size	0.22 x 0.22 mm^2	0.22 x 0.22 mm^2
SNR	10.08	7.64

Table 3-7. Images of an adult male zebra finch were acquired using a "RARE_8_bas" pulse sequence. Experiments aimed at testing the effects of zero filling, output size and reconstruction size on scan time, resolution and signal to noise ratio.

Because both acquisitions had a field of view of 1.40 x 1.40 cm^2 and identical reconstruction and output sizes, they had equally high resolutions as a result. Furthermore, the resolution of both acquisitions' resultant images was far improved in comparison to previous acquisitions with a zebra finch subject: pixel size was 0.22 x 0.22 mm^2 (Table 3-7, Table 3-6). The SNR for the first reconstruction method was much higher than the SNR for the second method that was tested, zero filling. This makes sense because the zero filled image had an acquisition matrix of 64 x 32 pixels. There is less signal per pixel collected in the 64 x 32 pixel acquisition matrix in comparison to the 32 x 32 pixel acquisition matrix used in the Acquisition 1, since both acquisitions had the same FOV. This was the cause of the decreased SNR. Moth methods had the same scan time, since 32 x 32 pixel and 64 x 32 pixel acquisition matrices have the same resolution in the spatial domain. As a result, these two methods, having the same RARE factors, collected the same

number of lines of k-space in the number of TRs. Collectively, the results from this experiment showed that both methods tested produced high resolution images in the minimum scan time. However, modifications to output and reconstruction size produce higher SNR images than zero filling.

In a second and final functional imaging experiment, eight sets of axial images were acquired. Four brain volumes out of the eight were scanned in silence, and 4 volumes were scanned with a conspecific song stimulus, which was projected using G-MAX 2000 Gateway external audio speakers. The experiment used a square 32 x 32 pixel acquisition matrix, an output matrix of 64 x 64 pixels and a reconstruction matrix of 64 x 64 pixels. Field of view (FOV) was decreased to 1.4 x 1.4 cm^2 to increase resolution and the FOV was centered on the brain using the ParaVision geometry editor (Fig. 3-16). These steps would ensure that the images would be more easily compatible with SPM 8, which is very sensitive to brain size, image origin and alignment.[20] Pixel size for the reconstructed images was 0.22 x 0.22 mm^2. These sets of images should be processed in SPM 8 in future work.

Figure 3-16. Axial image was acquired using a RARE_8_bas pulse sequence for functional MRI with symmetrical 0.22 x 0.22 mm^2 pixels. FOV was centered on the zebra finch brain.

Summary

It is clear that while EPI is capable of far more rapid image acquisitions, RARE has the potential for attaining far more acceptable image quality in comparison, largely because it is free of both distortions and signal loss. Likewise, a RARE pulse sequence can attain optimal image quality with a specified set of scanning parameters. A RARE factor of 8 is ideal, since it permits rapid imaging with minimal signal loss due to an extended effective TE, which allows for excess spin dephasing. A small matrix size, 32 x 32 pixels, increases SNR while decreasing scan time. To compensate for decreased resolution, output matrix size and reconstruction matrix size can be adjusted to 64 x 64 pixels each without sacrificing scan time. This is because the number of pixels in the acquisition matrix directly correlates to the number of lines in k-space required to form an image. Thus, an image with an acquisition matrix of 32 x 32 pixels requires half as many lines of k-space and therefore half the scan time in comparison to an image with a 64 x 64 pixel acquisition matrix size. However, in this case, the images were reconstructed post-acquisition to give a 64 x 64 pixel image. A very small field of view can also help center the brain in the image and leads to a decreased pixel size. However, because less signal is collected per pixel, small FOV sacrifices SNR. Additionally, because SNR significantly decreases with the number of averages, an intermediate number of averages is ideal. This option minimizes scan time, but not at the cost of image quality. A somewhat increased scan time is acceptable since a prolonged sound stimulus can also extend the BOLD response (Fig. 3-12).[9]

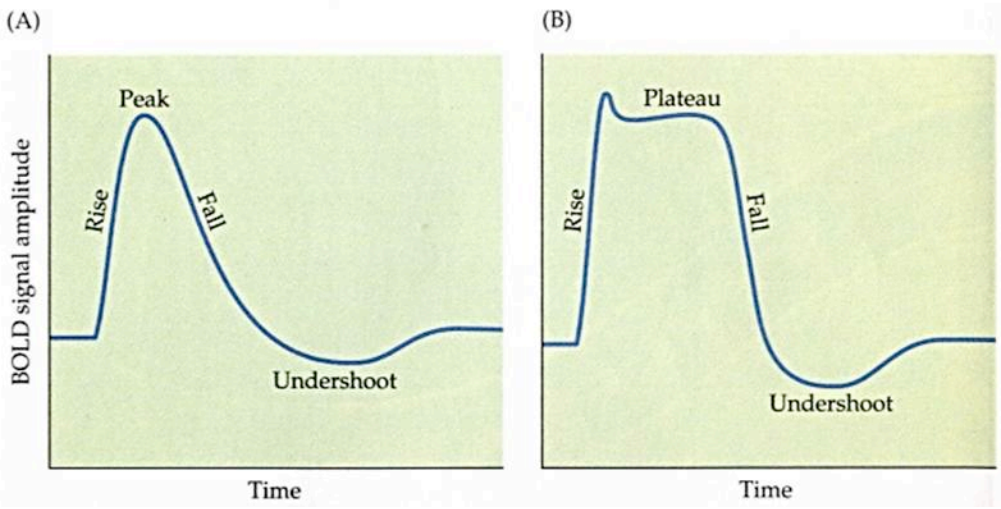

Figure 3-12.[9] The BOLD response (A) reaches a peak at about 5 seconds post-stimulus and (B) can be prolonged by an extended stimulus.

4 Conclusions and Future Work

The Fast Spin Echo pulse sequence RARE produces high-quality functional images within a scan time of 8 seconds, fast enough to capture the BOLD response. This scan time can be reduced at little expense to signal-to-noise (SNR) ratio and resolution by decreasing the number of averages, and decreasing matrix size while zero-filling or using an increased output size. When compared with the popular gradient echo pulse sequence, EPI, RARE produces images of equal resolution, without artifacts such as distortions or signal dropout. The determining factor for our choice in pulse sequence was the presence of artifacts, since only RARE appears to be able to generate accurate MR image representations of an avian subject.

Future work should focus on improving the quality of functional imaging results and implementing an improved protocol on isolate birds to study song learning.

- fMRI results can be improved by increasing the number of blocks per experiment to increase the overall sample size for analysis.
- Another possible way to improve the quality and reliability of the results would be to test the use of a non-magnetic speaker for in-magnet sound delivery. The use of a speaker inside the micro-MRI system could potentially improve the subject's ability to accurately perceive song over the loud gradient and radio frequency pulses implemented throughout imaging.
- It will also be important to study song learning in isolate birds, and later experiment with unanaesthetized animals to more accurately probe song learning and show whether anesthesia affects this process on the neuronal level.

- A last important step in improving outcomes for this study of vocal learning is to master the use of SPM. This would allow us to assess the efficacy of our external speakers in comparison to non-magnetic speakers. Ultimately, it will also permit us to interpret longitudinal studies of song learning in isolate birds.

References

1. Van Meir, V. *et al.* Spatiotemporal properties of the BOLD response in the songbirds' auditory circuit during a variety of listening tasks. *Neuroimage* **25,** 1242–1255 (2005).
2. Bolhuis, J. J., Okanoya, K. & Scharff, C. Twitter evolution: converging mechanisms in birdsong and human speech. *Nature Reviews Neuroscience* **11,** 747–759 (2010).
3. Van Ruijssevelt, L., Van der Kant, A., De Groof, G. & Van der Linden, A. Current state-of-the-art of auditory functional MRI (fMRI) on zebra finches: Technique and scientific achievements. *Journal of Physiology-Paris* (2012). doi:10.1016/j.jphysparis.2012.08.005
4. Lipton, M. L. *Totally accessible MRI: a user's guide to principles, technology, and applications*. (Springer, 2008). at <http://books.google.com/books?hl=en&lr=&id=39tDf449i4kC&oi=fnd&pg=PR7&dq=%22nodule+from+normal+liver+tissue.+In+an+effort+to+maximize+the%22+%22signal+between+tissues,+we+modulate+the+measured+signal+by+adjusting%22+%22of+the+MR%22+%22we+progress+in+our+understanding+of+MRI,+do+not+lose+sight+of+the%22+&ots=3Js8cF7RPi&sig=Rzg8zMsR_2Z6WEJqRWn0vk2jXPI>
5. Hashemi, R. H., Bradley, W. G. & Lisanti, C. J. *MRI: The Basics*. (Lippincott Williams & Wilkins, 2010).
6. Skoog, D. A. *Principles of instrumental analysis*. (Brooks/Cole : Thomson Learning, 1998).
7. Hornak, J. P. *The Basics of MRI*. (Interactive Learning Software, 2010). at <http://www.cis.rit.edu/htbooks/mri/inside.htm>
8. McRobbie, D. W., Moore, E. A., Graves, M. J. & Prince, M. R. *MRI From Picture to Proton*. (Cambridge University Press, 2006).
9. Huettel, S. A., Song, A. W. & McCarthy, G. *Functional Magnetic Resonance Imaging*. (Sinauer Associates, Inc, 2004).
10. Stroman, P. W. *Essentials of Functional MRI*. (CRC Press, 2011).
11. Poirier, C., Verhoye, M., Boumans, T. & Van der Linden, A. Implementation of spin-echo blood oxygen level-dependent (BOLD) functional MRI in birds. *NMR in Biomedicine* **23,** 1027–1032 (2010).
12. Jackson, G. D., Briellmann, R. S., Waites, A. B., Pell, G. S. & Abbott, D. F. Functional MRI. *Modern Magnetic Resonance* 1037–1050 (2006).
13. Chew, S. J., Mello, C., Nottebohm, F., Jarvis, E. & Vicario, D. S. Decrements in auditory responses to a repeated conspecific song are long-lasting and

require two periods of protein synthesis in the songbird forebrain. *Proceedings of the National Academy of Sciences* **92,** 3406–3410 (1995).
14. Moorman, S. *et al.* Human-like brain hemispheric dominance in birdsong learning. *PNAS* (2012). doi:10.1073/pnas.1207207109
15. Poirier, C., Boumans, T., Verhoye, M., Balthazart, J. & Van der Linden, A. Own-song recognition in the songbird auditory pathway: selectivity and lateralization. *The Journal of Neuroscience* **29,** 2252–2258 (2009).
16. Lee, S.-P., Silva, A. C., Ugurbil, K. & Kim, S.-G. Diffusion-weighted spin-echo fMRI at 9.4 T: microvascular/tissue contribution to BOLD signal changes. *Magnetic resonance in medicine* **42,** 919–928 (1999).
17. Poirier, C. & Van der Linden, A. M. Spin echo BOLD fMRI on songbirds. *Methods in Molecular Biology (Clifton, NJ)* **771,** 569–576 (2011).
18. Huang, S. A Magnetic Resonance Study of the GCPII+/- Mouse Model. (2012).
19. Lipton, M. L. *Totally Accessible MRI: A User's Guide to Principles, Technology and Applications*. (Springer, 2008).
20. Rorden, C. Sample fMRI Event-Related Design Analysis using SPM. *MRIcron Index* at <http://www.mccauslandcenter.sc.edu/CRNL/sw/tutorial/html/eventspm.html>
21. Hermans, E. J. SPM8 Starter's Guide. (2002).

Appendices

Appendix A: Guide to Sound Stimulus Recording and Construction

Novel sound stimuli shall be recorded using 2011 SP1 (32-bit) 6-channel detect-record v2.0 software in conjunction with a SHURE 93 recording system in conjunction with a NADY Audio PRA-8 8 channel mic pre-amplifier. The following steps shall be followed when preparing the 6-channel detect-record v2.0 program: Once the software has opened, the window shown in Figure A-1 will appear. This program is designed to selectively recognize and record zebra finch song while ignoring calls and background noise. The two boxes at the top of the screen will provide graphical representations of the frequency and amplitude of all songs recorded in birds' soundproof isolation coolers.

The text in box A of fig. A-1 and all subsequent headings denote the soundproof isolation cooler number at which each recording is being collected (box A corresponds to cooler 0). In box B, the user must enter the tag color and ID number of the bird being recorded in the corresponding cooler. The entry must consist of a three-letter abbreviation for the bird's tag color followed by the ID number. (Color and ID are not separated by a space. For example, Red86, Pur04, Blu54.) A path, as shown in box C of Figure A-1, should be designated as "C:\\SongRecording\Color##," for which Color## is the bird's tag color and ID as written in box B. When beginning a new set of recordings for a new animal, the "Current Record Index" (box D) should be manually set to 0. To ensure song recordings are saved, click button E in fig. A-1 labeled "Save Song Files." To begin recording, press button F in the upper left corner of the screen.

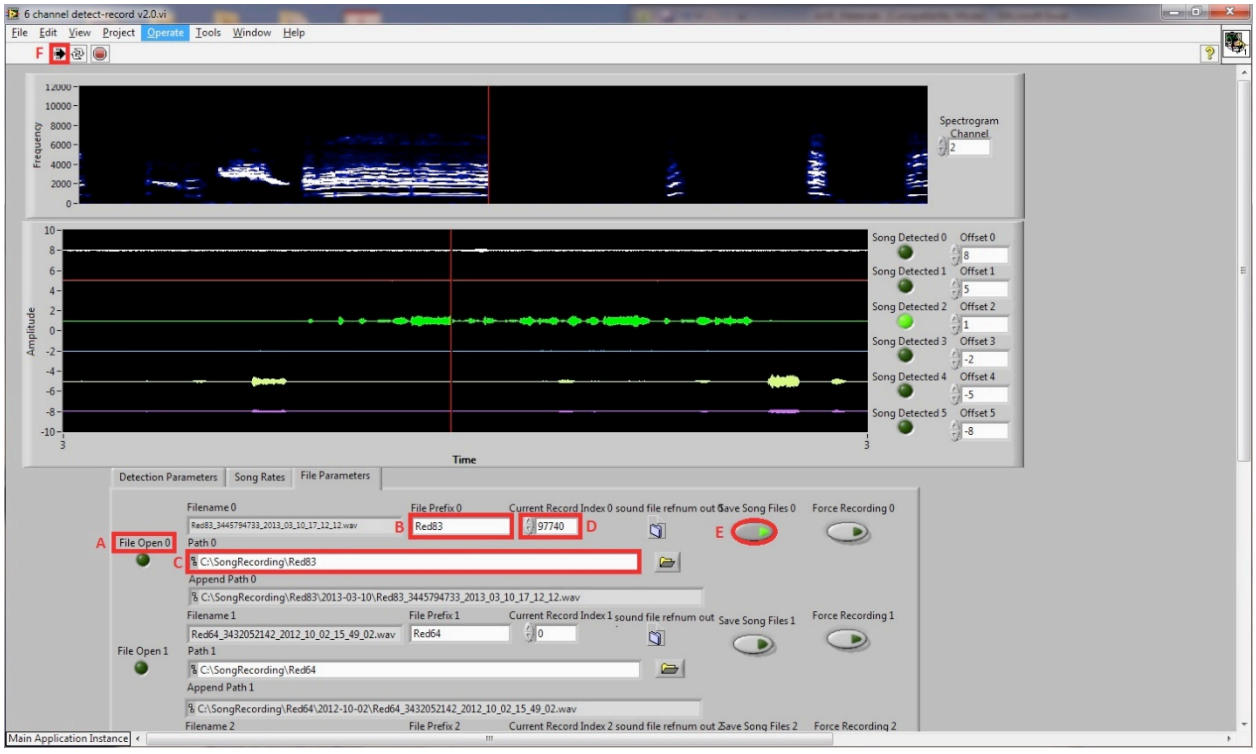

Figure A-1. Screenshot of the 2011 SP1 (32-bit) 6-channel detect-record v2.0 main screen.

Once raw recordings have been made, sound files for each bird can be found in the path designated by fig. A-1, box C. The first step for constructing usable song stimuli is to listen to those recordings. Select the sound files with the best clarity and whose duration is between 2 and 4 seconds to construct a stimulus.

Use the computer program Praat to construct song stimli for functional imaging. Once the program has been started, load a sound file by clicking the "Open" tab in the "Praat Objects" window and selecting "Read from file" (Fig. A-2). If you are working with a very long song file, select the "open long sound file" option (Fig. A-2). Once you load the sound file, it will appear in the "Objects" workspace in the "Praat Objects" window. Then, add a second of silence after the first sound clip by selecting "New," then "Sound," then "Create Sound from formula" (Fig. A-2). In the window that appears, type 0 in the "Formula" textbox and adjust the length of the silence by entering the number of seconds in the "End time(s)" textbox (Fig. A-3). Then click "OK." The silent period will then appear in the "Objects" workspace in the "Praat Objects" window below the song file. Continue adding the alternating song files and one second periods of silence until the entire list of objects in the workspace spans the desired period of time. (This period generally correlates to the duration of a functional image acquisition.)

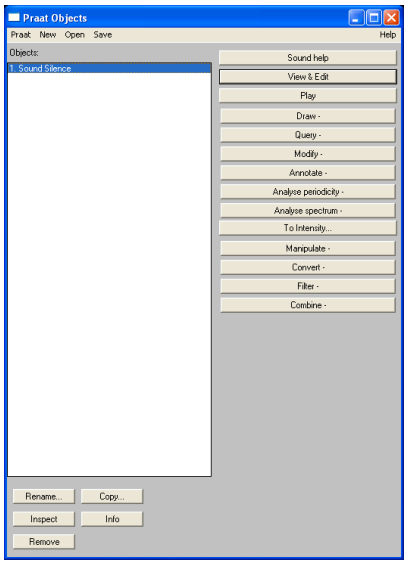

Figure A-2. "Praat Objects" window.

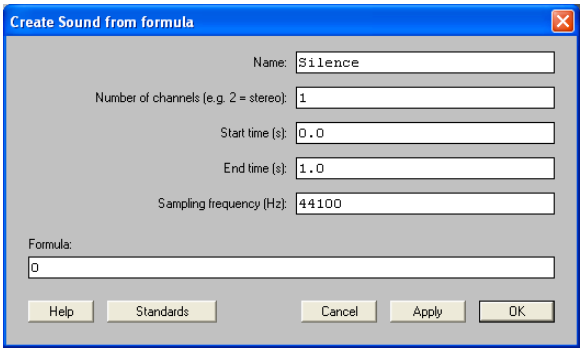

Figure A-3. To create period of silence, type "0" in the formula textbox of the "Create Sound from formula" window. Adjust the duration of the silence by entering a numerical value in the "End time (s)" textbox.

To combine the sound clips into one file, highlight all of the clips and select "Combine," and then "Concatonate" in the tool bar of the "Praat Objects" window (Fig. A-2). Then, listen to the full sound file. If necessary, the stimulus can be amplified. To do so, select "Modify," then "Multiply" in the tool bar of the "Praat Objects" window (Fig. A-2). In the window that appears, enter a multiplication factor in the text box (Fig. A-3). Click "OK." Then, save the new sound file as a .wav file.

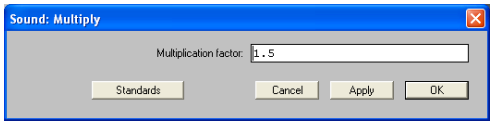

Figure A-3. Enter a numerical value in the text box of the "Sound: Multiply" window to amplify your sound file by that factor.

Appendix B: Guide to Speaker Assembly

The following speaker models were ordered from All Electronics Corporation for sound stimulus delivery in the micro-MRI system: 20 mm, 150 Ω speaker (0.79" diameter x 0.1" thick); 300 Ω, 40 mm speaker (40 mm diameter x 8 mm thick); 50 mm, 4 Ω speaker (50 mm diameter x 10 mm thick; prepared with 5" leads) (Fig. A-4).

Figure A-4. Three speaker models were ordered for sound stimulus delivery. (A) A 20 mm, 150 Ω speaker, (B) a 300 Ω, 40 mm speaker, and (C) a 50 mm, 4 Ω speaker, all of which were ordered from All Electronics Corporation.

The first preparatory step was to remove the magnet from each speaker. This step will allow the speakers to operate safely within the bore of the MRI (Fig. A-5).

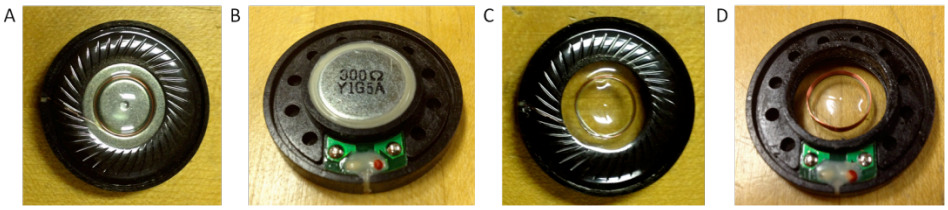

Figure A-5. A 300 Ω, 40 mm speaker is shown (A, B) before and (C, D) after its magnet is removed.

Next, electrical wires were fused to the solder terminals of each speaker using a lead-based solder (Fig. A-6).

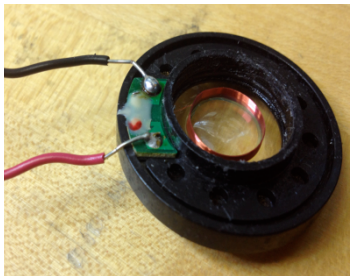

Figure A-6. A 300 Ω, 40 mm speaker is shown with electrical wires soldered to its solder terminals.

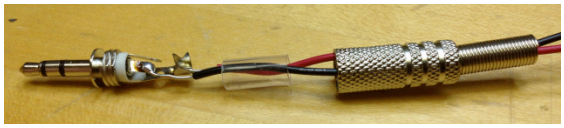

Figure A-7. Electrical wires are shown soldered to a disassembled 3.5 mm metal plug.

The other ends of those wires were soldered to the terminals of a stereo 3.5 mm metal plug (Fig. A-7). (Metal plugs were also purchased from All Electronics Corporation.) A fully assembled speaker is shown in Figure A-8.

Figure A-8. A fully assembled 300 Ω, 40 mm speaker.

Appendix C: Guide to Postprocessing (Adapted from the SPM 8 Manual)

Open Matlab and in the command line, type "spm fmri." It will look like this:

```
>> spm fmri
```

SPM is very sensitive to the origin set as the initial alignment between the image and normalization template.[20] (The program assumes that the origin is set at the anterior commissure.) These next few steps will help ensure that the origin is properly set. First, on the SPM8 Menu, select "Display," and then choose your highest resolution image.

Reorientation

The graphics window will appear on the screen, displaying three views of your three-dimensional data (Fig. A-9). First, it is important to enlarge the images to a size viewable in SPM, which assumes that all imaging data is from a human-sized brain. To increase the size of the images, start by changing the value in the "resize (x)" text box to 3. Likewise, change the "resize (y)" and "resize (z)" values to 3 so that the image will be enlarged symmetrically (Fig. A-9).

To set the origin, manipulate the "right," "forward" and "up" values. When these values are altered, the blue cross hairs will change position in the x, y and z planes. Since bird brain anatomy is different from human brain anatomy, center the crosshairs such that they evenly split the two hemispheres in the coronal and horizontal views. In the sagittal view, the crosshairs should be positioned in the lower third, and slightly rostral to the center of the brain (Fig. A-9). This location would be spatially analogous to the anterior commissure in humans. It is also possible to rotate the brain by changing the numerical values of the "pitch," "roll" and "yaw" text boxes (Fig. A-9).

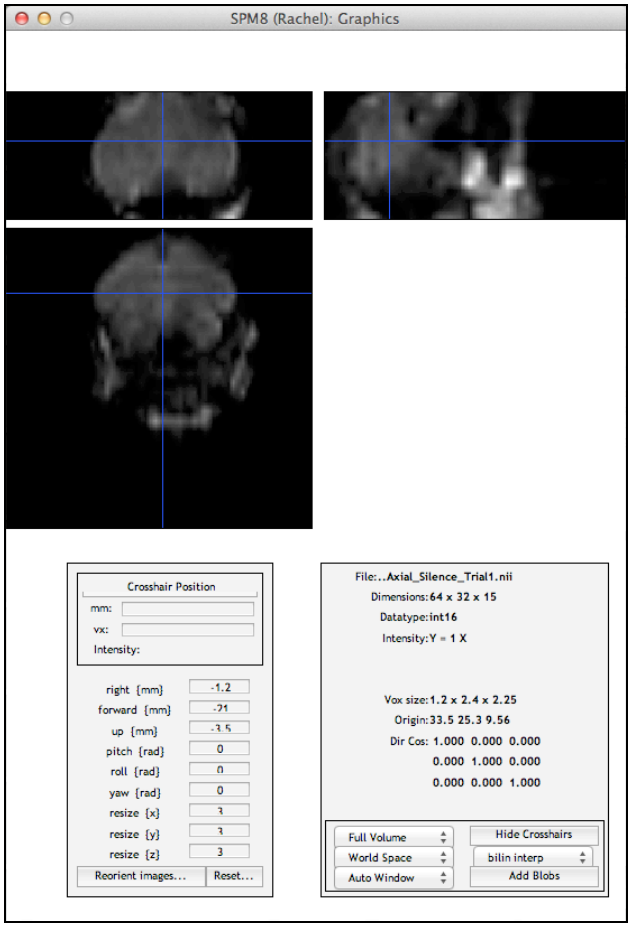

Figure A-9. Image size, shape and origin can be modified in the Graphics window by choosing "Display" in the SPM8 Menu.

Still in the SPM8 Graphics window, click "Reorient Images" to apply these changes to the origin and rotation to the entire set of images. In the window, "Images to reorient," select all of the images you intend to process, including the template image you used for reorientation. When you are finished, click "Done," and the entire set of images will be reoriented such that they all contain the same origin and orientation in space.

Realignment

In the SPM8 Menu's *Spatial pre-processing* window, click the "Realign" tab and select the option "Realign (Est & Res)" from the pulldown menu. Then, in the batch editor window highlight data, and then select "New Session." Highlight the new "Session" option and select "Specify Files." Choose all of the imaging data to be processed. Next, save the job (click the floppy disk icon in the upper left hand corner) as realign.mat in the same directory as the rest of your images. Click the green "run" arrow in the upper left hand corner adjacent to the "save" button to begin realignment. Data for the realignment should appear in the SPM8 Graphics window. An example is shown in Figure A-10.

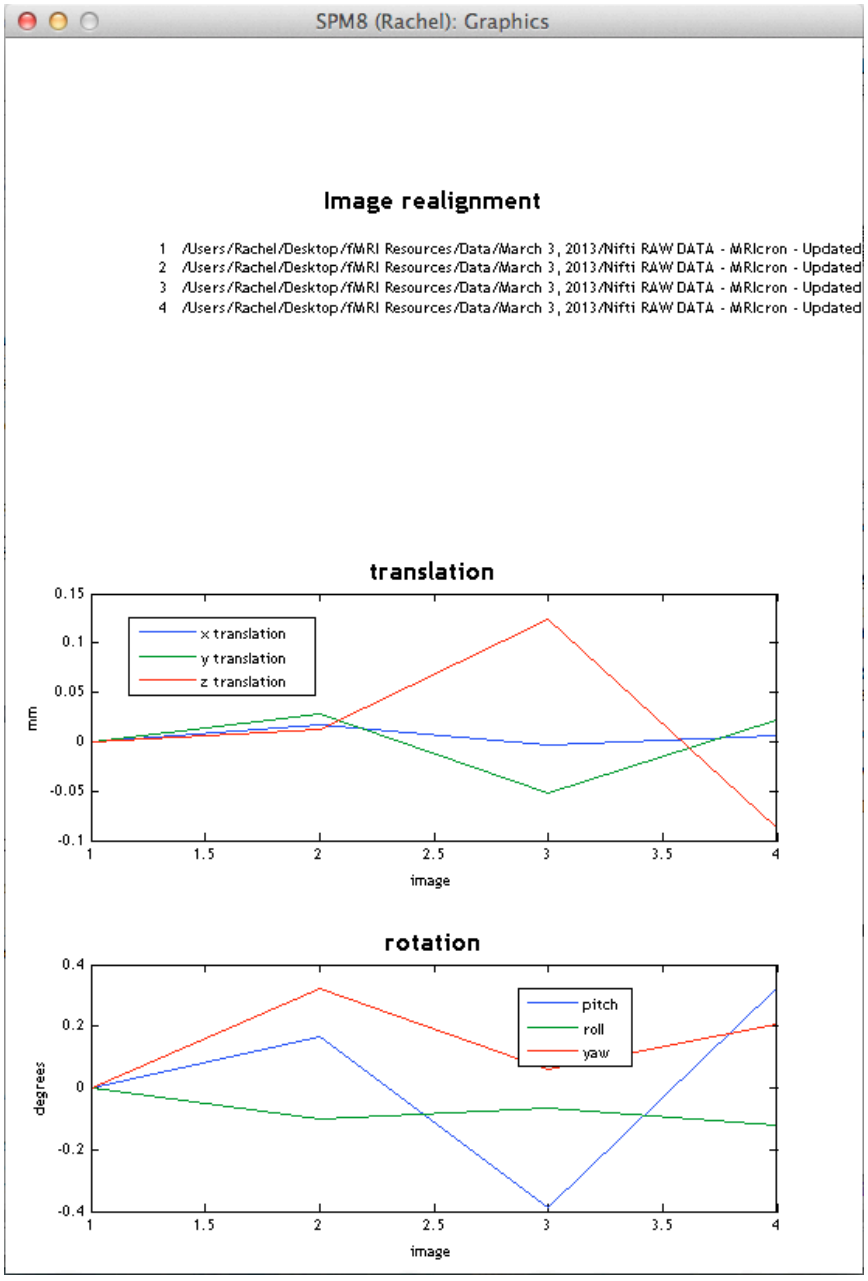

Figure A-10. Realignment data, as shown in the Graphics window.

Coregistration

Exit the batch editor and return to the SPM8 Menu. Then select "Coregister (Estimate)" from the "Coregister" pull-down menu. When the batch editor window reappears, highlight "Reference Image" and select the mean fMRI scan that was created during the realignment step. (This scan will appear in the same directory as your original images and begin with the word "mean.") Highlight "Source Image" and select the structural image that you used previously during realignment. Then, click the save button and save the file as coreg.mat. Complete this step by pressing the run button (green arrow).

Segmentation

During segmentation, SPM will create gray and white matter images, as well as a bias-field corrected structural image. To start, select "Segment" in the SPM8 Menu *Spatial pre-processing* window. When the batch editor appears, highlight "Data" and then select the previously designated anatomical image. Then press "Done." Save the file as segment.mat and press run.

Normalization

Select "Normalise (write)" from the Normalise pulldown menu. In the batch editor, highlight "Data" and then select "New: Subject." Highlight "Parameter File" and select the file ending in "_seg_sn.mat" that was created during segmentation and press "Done." Next, highlight "Images to Write" and select all realigned functional images (files will start with the letter "r"). Then, press the save button, and save the job as "normalise.mat." Press run.

In order to later superimpose the subject's activations on its own anatomy, select "Normalise (write)" once more. Highlight "Data," then select "New Subject" Highlight "Parameter File" and once again select the file ending in "_seg_sn.mat" that was created during segmentation and press "Done." Then, highlight "Images to Write," and then select the image file with the prefix "m." This is our bias-corrected structural image. Under "Writing Options," select "Voxel Sizes," and then click "Edit Value." Change the voxel size matrix from [2 2 2] to a matrix corresponding to the original resolution of the images. Save the job as norm_struct.mat and press the run button.

Smoothing

This step is not strictly necessary if you are only interested in Bayesian analysis. Smoothing is not recommended if you are interested in very small features.[21]

Start by pressing the Smooth button. Then click on "Images to Smooth," to select the spatially normalized files from their designated directory. (These files should all start with the letters "wr" followed by their original file names.) Highlight "FWHM" and change [8 8 8] to a matrix more suitable to your data set. It is conventional to choose a Full Width at Half Maximum (FWHM) that is twice the size of the voxels in the image.[21] For example, if your voxel size is 2 x 2 x 1 mm^3, then choose a FWHM of [4 4 2]. This would mean that SPM will smooth the data 4 mm in the x and y directions and 2 mm in the z direction. Finally, save the job as smooth.mat and press Run.

Model Specification

Choose "Specify 1st- level" from the "Model specification, review and estimation" window in the SPM8 Menu. Under "Timing parameters" in the batch editor,

highlight “Units for design” and select “Scans.” Highlight “Interscan interval” under “Timing Parameters” and enter the TR of the scans used in the experiment. Next, highlight “Data & Design” and select “New: Subject/Session.” Under the “Subject/Session” in the Current Module, highlight “Scans” to select the images you are using in your experimental paradigm. Once you have selected all the images, press “Done.”

Highlight “Conditions” and select “New: Condition” from the “Current Item” window. Under “Condition” in the “Current Module” window, highlight “Name” to choose a name for your “ON” condition. For example, this condition could be named “active,” or “song.” If there are multiple “ON” conditions in the experiment, for example, tutor song, conspecific song, and white noise, multiple conditions must be created in this step. Highlight “Onsets” and enter a matrix representing the scans *after* which stimulus onset began. For example, say there are 12 total scans representing alternating periods of rest and song. Blocks consist of 3 scan each, and begin with rest. The following matrix would be entered in “Onsets”: [3, 9]. Highlight “Directory” and then click “Select files” to select the directory in which you wish to write this job. Finally, save the job as specify.mat and press Run. Your design matrix will appear in the SPM8 Graphics window (Figure A-11).

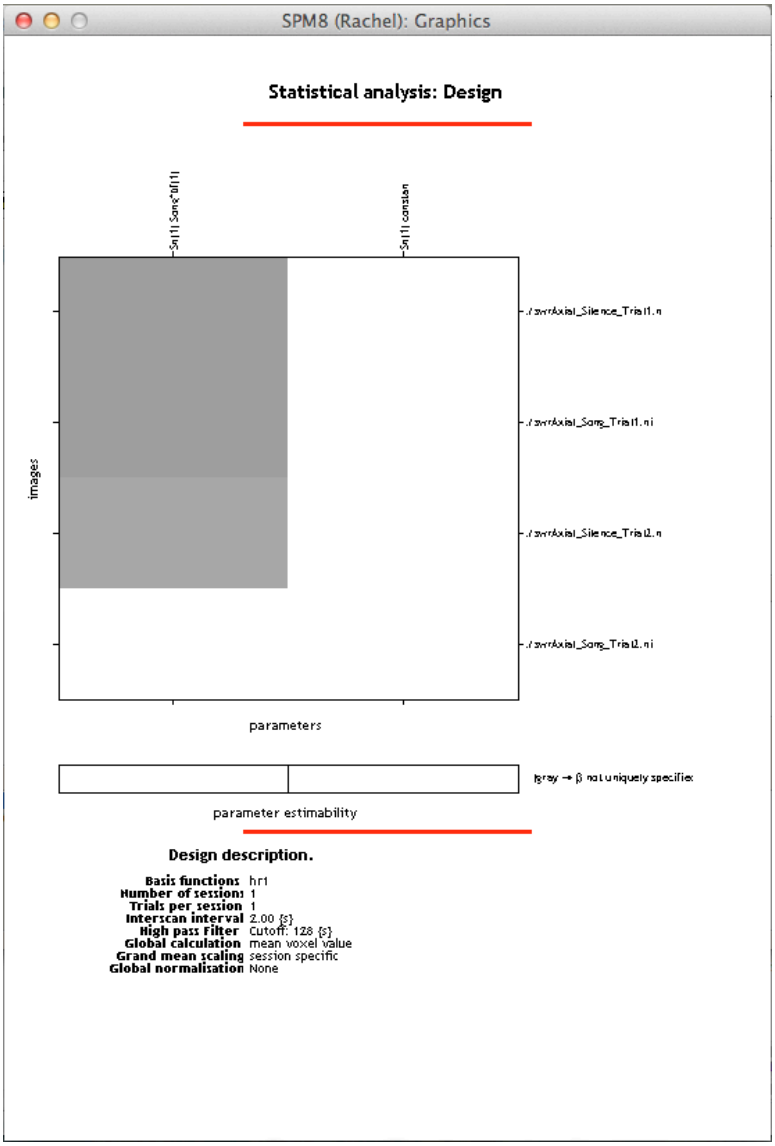

Figure A-11. The design matrix will appear in the SPM8 Graphics window after first level specification is completed.

Estimate

Press "Estimate" in the "Model specification, review and estimation" window of the SPM8 Menu. Highlight "Select SPM.mat," and then select the SPM.mat file saved in the directory specified in the "Model Specification" section. Then, save the job as estimate.job and press Run.

Inference

Press "Results" in the "Inference" window of the SPM8 Menu and select the same SPM.mat file in the directory specified in the "Model Specification" section.

Contrast Manager

When the "Contrast manager" window appears, select "t-contrast," to produce t-test statistical results. Then select "Define new contrast…" For a one-sided t-test, specify "song > rest" in the "name" text box and the number "1" in the "contrast" text box. ("song" is the name of your "ON" condition chosen during "Model Specification.") Ensure that "t-contrast" is the selected "type." Press OK. Then, highlight your recently created contrast name in the "SPM contrast manager" window and press "Done."

Results

Next, the "SPM8: States: Results" window will activate and prompt you with an option to "apply masking." Select "none." When a "title for comparison" appears in the same window, check that the title matches your contrast name, i.e. "song > rest," and press enter. For "p value adjustment control," select "FWE." A p value will then appear in the window. For a 95% confidence interval, let the p value (FWE) be 0.05 and press enter. Let the extent threshold be 0 and press enter. In the graphics window, a Maximum Intensity Projection (MIP) of the newly generated statistical map will appear (Fig. A-12).

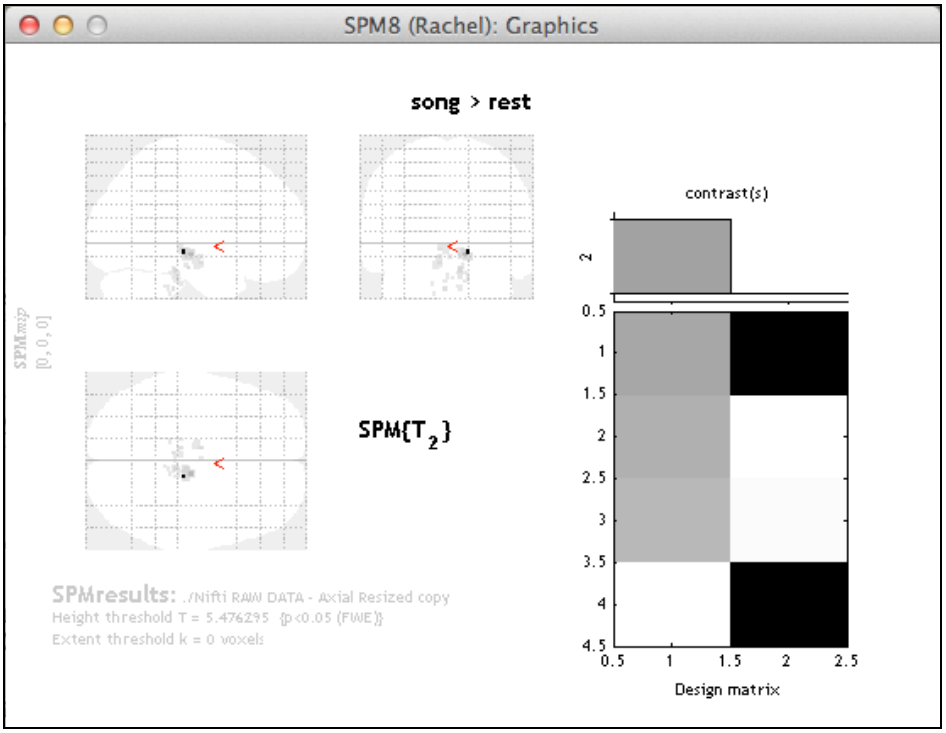

Figure A-12. Maximum Intensity Projection of a statistical activation map representing the auditory BOLD response "song > rest" for a zebra finch subject.

Overlays

In the "Display" section of the "SPM8: SPM{T}: Results" interactive window, the "overlays" dropdown menu provides three choices for the visualization of a newly created activation map:

a. The "slices" option displays three adjacent axial slices. When this option is selected, SPM will display a new window, "Select image for rendering on." To superimpose a subject's activations on its own anatomy, select the bias-corrected anatomical image starting with the prefix "wm."

b. The "sections" option will display three intersecting sagittal, coronal and axial slices. Once again, SPM will display a new window, "Select image for rendering on." To superimpose a subject's activations on its own anatomy, select the bias-corrected anatomical image starting with the prefix "wm."

c. The "render" option will display the activation map on a 3D volume rendered brain. For this type of overlay, we must first create a rendering using the white and gray matter segmented images: Select "Normalize (Write)" from the SPM 8 Menu. Under "Data," select "New: Subject." Then highlight "Parameter File" and select the file ending in "_seg_sn.mat." Highlight "Images to Write" and select the two images beginning in "c1" and "c2." Press Run. Next, in the "SPM for functional MRI" window in the SPM8 Menu, under the "Render" dropdown menu select "Xtract Surface." In the "Select images" window that pops up, choose the two newly normalized files starting with the prefixes "wc1" and "wc2." In the interactive SPM8:Surface menu, under the "Save…" dropdown menu, select the default option, "Save Rendering and Surface" to produce the 3D rendering.